ABSTRACT

Title of Document: MEMBRANE MODELS OF E. COLI CONTAINING CYCLIC MOIETIES IN THE ALIPHATIC LIPID CHAIN

Kunal Pandit, Master of Science, 2011

Directed By: Prof. Jeffery B. Klauda
Department of Chemical & Biomolecular Engineering

Most molecular dynamics (MD) simulations of bacterial membranes simplify the membrane by composing it of only 1-palmitoyl-2-oleoyl-*sn*-glycero-3-phosphoethanolamine (POPE) or in some cases with1-palmitoyl-2-oleoyl-*sn*-glycero-3-phosphoglycerol (POPG) as well. However, an important constituent of bacterial membranes are lipids with a cyclopropane ring in the acyl chain. We developed a complex membrane that reflects the diverse population of lipids within *E. coli* cytoplasmic membranes, including cyclic lipids. Differences between the deuterium order profile of cyclic and monounsaturated lipids are observed. Furthermore, inclusion of the ring decreases the surface density of the bilayer and produces a more rigid membrane as compared to POPE/POPG membranes. Additionally, the diverse acyl chain length creates a thinner bilayer which better matches the hydrophobic thickness of *E. coli* transmembrane proteins. We believe the complex membrane is more accurate and suggest the use of it in MD simulations rather than simple membranes.

Membrane Models of *E. coli* Containing Cyclic Moieties in the Aliphatic Lipid Chain

By

Kunal Pandit

Thesis submitted to the Faculty of the Graduate School of the
University of Maryland, College Park, in partial fulfillment
of the requirements for the degree of
Master of Science
2011

Advisory Committee:
Professor Jeffery Klauda, Chair
Professor Panagiotis Dimitrakopoulos
Professor Srinivasa Raghavan

DEDICATION

This thesis is dedicated to my parents, Joan and Praveen. Thank you for providing me your love, your support, and everything I have ever needed and more.

ACKNOWLEDGMENTS

I would like to acknowledge the guidance of Dr. Jeffery Klauda, who pushed me in the correct direction at every step of this project. I would also like to thank him for helping me attend AIChE and BPS this year, where I was just completely fascinated.

TABLE OF CONTENTS

LIST OF TABLES

LIST OF FIGURES

LIST OF ABBREVIATIONS

ABNR	Adopted Base Newton-Raphson
AMPS	Antimicrobial Peptides
C36c	modified CHARMM36 force field
CED	Compression Energy Density
DIMS	Dynamic Importance Sampling
DPPG	1,2-dipalmitoyl-*sn*-glycero-3-phosphoglycerol
FA	Fatty Acids
FF	Force Field
GC	Gas Chromatography
IM-EX	Implicit-Explicit membrane
LC	Liquid Chromatography
MD	Molecular Dynamics
MS	Mass Spectrometry
NMR	Nuclear Magnetic Resonance
NPAT	isothermic-normal isobaric ensemble
NPT	isothermic-isobaric ensemble
OPM	Orientations of Proteins in Membranes database
OSPE	1-oleoyl-2-palmitoleoyl-*sn*-glycero-3-phosphoethanolamine
PBC	Periodic Boundary Conditions
PDSPC	l-palmitoyl-2-dihydrosterculoyl-*sn*-glycero-3-phosphocholine
PDSPE	l-palmitoyl-2-dihydrosterculoyl-*sn*-glycero-3-phosphoethanolamine
PE	Phosphoethanolamine
PG	Phosphoglycero
PME	Particle Mesh Ewald
PMPE	1-palmitoyl-2-*cis*-9,10-methylene-hexadecanoic-acid-glycero-*sn*-3-phosphoethanolamine
PMPG	1-palmitoyl-2-*cis*-9,10-methylene-hexadecanoic-acid-glycero-*sn*-3-phosphoglycerol
PSPG	1-palmitoyl-2-palmitoleoyl-*sn*-glycero-3-phosphoglycerol
POPC	1-palmitoyl-2-oleoyl-*sn*-glycero-3-phosphocholine
POPE	1-palmitoyl-2-oleoyl-*sn*-glycero-3-phosphoethanolamine
POPG	1-palmitoyl-2-oleoyl-*sn*-glycero-3-phosphoglycerol
QM	Quantum Mechanics
QMPE	1-pentadecanoyl-2-*cis*-9,10-methylene-hexadecanoic-acid-*sn*-glycero-3-phosphoethanolamine
SA	Surface Area per lipid
S_{CD}	deuterium order parameters
SD	Steepest Descent
THM-GC	Thermally assisted Hydrolysis Methylation-Gas Chromatography

CHAPTER 1 BACKGROUND

1.1 *E. coli* Membranes

Cellular membranes provide a vital and protective barrier between the extracellular and intracellular environment, while allowing transport of specific molecules across the bilayer. The main constituents of cytoplasmic membranes are glycerophospholipids, which contain a polar head group and two hydrophobic fatty acids (FA). These lipids are arranged in two layers of flat sheets to form a lipid bilayer which encompasses the cell.

The complexity of biological membranes is immense due to a heterogeneous mixture of various biomolecules. The simplest description would just be a homogenous lipid bilayer. A more realistic model would include a variety of lipids, sterols, and membrane proteins. Furthermore, a complete portrayal would have glycosylated lipids, proteins, and cytoskeleton components. Understandably, a complete description is impractical to use in most studies, but a simple homogeneous lipid bilayer may be an insufficient model.

An accurate representation of the membrane environment is important because lipid-protein interactions are essential to membrane protein function and orientation. Loss of these interactions may destabilize and inactivate the protein. Even substituting the lipid environment with detergents may be inadequate as lost protein functionality has been experimentally observed (Popot 2010). Lipids may also play an integral role in a protein's mechanism. Krämer and Ziegler (Krämer and Ziegler 2009) have crystallized a structure of BetP, a bacterial integral membrane protein, where a lipid interaction aids in regulating its function. Lensik et al. (Lensink, Govaerts, and Ruysschaert 2010) found that 1-palmitoyl-2-oleoyl-*sn*-glycero-3-

phosphoethanolamine (POPE) mediated a salt bridge involved in proton gradient-sensing of the integral membrane protein lactose permease. The function of mechanosensitive channels, such as MscS and MscL are controlled by the surface tension in the lipid bilayer (Wiggins and Phillips 2005), which can depend strongly on local composition.

Model membranes consist of a simple lipid bilayer composed of the most relevant lipids. Experimentally, unilamellar vesicles are formed from either a distribution of naturally derived lipids (Dalrymple et al. 2011) or a mixture of specific lipids and sterols. In explicit molecular dynamic (MD) simulations, membranes usually consist of only one or two different lipids and may include sterols. Recently, detailed membranes consisting of a more diverse lipid population has been developed to model Chlamydia and Yeast membranes (Jo et al. 2009; Lim and Klauda 2011). With MD simulations of bacterial membrane proteins, it is common to use a membrane consisting of only POPE (Alhadeff et al. 2011) and in some cases in combination with 1-palmitoyl-2-oleoyl-*sn*-glycero-3-phosphoglycerol (POPG) lipids. This is due to the ease of generating such a membrane, for example through CHARMM-GUI (Jo et al. 2008). Investigators conveniently focus their efforts on studying the protein, leaving the membrane as an afterthought. However, the composition of bacterial membranes varies depending on the bacterial species, strain, nutrients, and growth phase (Morein et al. 1996).

1.2 Molecular Dynamics

1.2.1 Introduction

Studying biological systems at the molecular level is necessary to understand structure/function relationships, characterize/quantify molecular interactions/energetics, and gain insight into bulk properties. Experimentally, there are a great number of x-ray crystal structures,

nuclear magnetic resonance (NMR) solution structures, and biochemical structural/functional/binding assays. However, there is usually a lack of dynamics and/or detail at the molecular level. Molecular dynamics (MD) has been used as a tool to bridge gaps and provide further information lacking from experimental studies. The application of MD to biological systems has grown over the decades with ever improving force fields and computational resources.

In very broad terms, a MD simulation calculates the potential energy, *U*, from a force field (FF) as a function of the 3-dimensional structure, $\vec{R}$, and then integrates the equations of motion (Eq. 1-1) for each particle in the system where $\vec{R}_i$ is the position of the particle, $\vec{F}_i$ is the force on the particle, and m_i is the mass of the particle. The FF usually consists of intramolecular (bonds, angles, and dihedrals) and nonbonded (electrostatics and van der Waals) terms (See Eq. 1-2). The force on each particle is found from the negative gradient of the potential energy and used to integrate the equation of motion. It can be integrated using a number of finite difference methods where position and velocities are approximated by Taylor series expansion (Leach 2001).

$$\frac{d^2\vec{R}_i}{dt^2} = \frac{\vec{F}_i}{m_i} \qquad (1\text{-}1)$$

$$U(\vec{R}) = \sum_{bonds} K_b(b - b_0)^2 + \sum_{angles} K_\theta(\theta - \theta_0)^2 + \sum_{dihedrals} \sum_{j} K_{\varphi,j}\left(1 + \cos\left(n_j\varphi - \delta_j\right)\right) + \sum_{nonbonded\ pairs\ i,j} \varepsilon_{ij}\left[\left(\frac{R_{min,ij}}{r_{ij}}\right)^{12} - \left(\frac{R_{min,ij}}{r_{ij}}\right)^{6}\right] + \sum_{nonbonded\ pairs\ i,j} \frac{q_i q_j}{\varepsilon_D r_{ij}} \quad (1\text{-}2)$$

1.2.2 Intramolecular FF

Intramolecular potentials describe interactions of atoms within a molecule. Harmonic potentials are used for the bond and angle energy terms, where deviations from a reference point incur an energetic penalty. As shown in Eq. 1-2, b is the bond length, θ is the valence angle, and the relevant FF parameters are the Urey-Bradley force constant, K_b, the equilibrium bond length, b_0, the valence angle force constant, K_θ, and equilibrium valence angle, θ_0. The dihedral term is represented by a cosine series expansion where multiple minimum dihedral angles, φ, can exist. For each cosine term, j, the relevant FF parameters are the dihedral force constant, K_φ, multiplicity (number of minimums), n, and phase angle, δ. Generally bond stretching requires more energy for significant deformation than angle bending. Torsions about the dihedral require less energy. Originally the dihedral term had physical meaning, but is now used as a correctional term for the internal potential and molecule conformation since the use of nonbonded terms for 1-4 interactions.

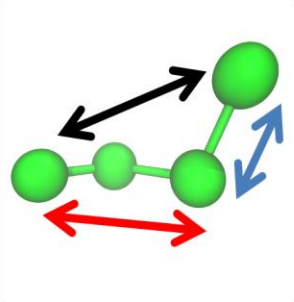

Figure 1.1 Intermolecular interactions. 1-2 interactions (*blue*) are between bonded atoms. 1-3 interactions (*red*) are between atoms separated by 1 atom. 1-4 interactions (*black*) are between atoms separated by 2 atoms.

1.2.3 Nonbonded FF

Nonbonded potentials in their most basic form, describe interactions between an atom and every other atom in the simulation and are the most computationally expensive calculations performed. However with the CHARMM FF and most other potentials, the 1-2 or 1-3 interactions are not included. The two nonbonded energy terms are van der Waals and electrostatic interactions. They are modeled as a function of some inverse power of the distance. Several other computational techniques are also employed to reduce costs.

Van der Waals interactions may be broken into two parts, attractive and repulsive. Attractive forces are based on a Drude model, related to induced dipole-dipole interactions, which predicts dispersal interactions to vary as $1/r^6$ (Leach 2001). Repulsive forces prevent atoms from occupying the same space, so small decreases in distance between atoms at short range produce very large increases in energy. For computationally convenience, the repulsive term is just the square of the attractive term. Thus a Lennard-Jones 12-6 function is used where r_{ij} is the distance between atom i and atom j, and the relevevant FF parameters are the Lennard-Jones well depth, ε_{ij}, and the minimum interaction distance, $R_{min,ij}$. In the CHARMM FF, the Lennard-Jones well depth and minimum interaction distance are developed for each atom type so

that ε_{ij} may be computed as the geometric mean, $\varepsilon_{ij} = \frac{1}{2}\sqrt{\varepsilon_i + \varepsilon_j}$, and $R_{min,ij}$ may be computed as the arithmetic mean, $\left(R_{min,i} + R_{min,j}\right)/2$.

To reduce computational time van der Waals interactions are not calculated for atoms separated by a certain cut-off radius. Since van der Waals interactions decay $\sim 1/r^6$ this is a good approximation. However, for a stable simulation, discontinuities in the potential should be avoided. In the MD simulation programs, CHARMM (B. R. Brooks et al. 2009) and NAMD (J. C. Phillips et al. 2005), a switching function (force- or potential-based) is implemented at a cut-on radius that smoothly brings the interaction to zero at the cut-off radius. Furthermore, the first and second derivatives of the switching function are 0 at the cut-on and cut-off radii. Since, calculating the distance between all atoms would negate gains in computational time with cut-offs, a nonbonded neighbors list is kept. An atom's neighbors are the atoms which are within a distance slight larger than that of the cut-off radius. They do not change significantly for 10-20 time steps. Thus, van der Waals interactions are only calculated for relevant pairs of atoms which are chosen from a nonbonded neighbors list that is regularly updated (Leach 2001).

Electrostatic interactions are modeled using Coulomb's Law where ε_D is the dielectric constant, set to 1 which corresponds to the permittivity of vacuum, and the relevant FF parameters are the partial charges of atoms i and j, q_i and q_j. Electrostatic interactions are calculated by brute summation for the central cell, but contributions from images are calculated using Particle Mesh Ewald (PME) (Darden, York, and Pedersen 1993). In Ewald summations, interactions with images are summed over by taking into account that image cells are an integer number of cell box lengths farther. The first step in PME is to replace the system of point charges and continuous coordinates with a grid based charge distribution. Next the summation of

charge-charge interactions over all images is split into two summations, one in real space and the other in reciprocal space, with the use of the complementary error function and error function respectively. In the real space summation, only the central box is considered and discrete charges in the mesh are surrounded by Gaussian charge distribution of equal but opposite magnitude and width κ (input by user). The neutralizing distributions are situated on lattice positions and integrate to zero. In the reciprocal space summation, to counteract charge distribution from the first part, a second opposite charge distribution is added to the system including images. The second summation considers long range interaction which converges rapidly in reciprocal space and is computed with the fast Fourier transform (Leach 2001). It is important to note that PME requires the central cell charge to be neutral. In NAMD, local force components are computed every time step, but long range force components, i.e. long range electrostatic interactions, can be computed every *h* time steps because they vary slowly. To more closely match CHARMM simulations, PME was calculated at every time step.

1.2.4 Periodic Boundary Conditions

Periodic boundary conditions (PBC) are necessary in MD simulations to circumvent artifacts that would arise from wall effects. With simple cubic PBCs, the central box is surrounded by 26 images on all sides, edges, and faces. As a molecule diffuses out of the central box on one side it is translated back into the central box on the opposite side. Care is also taken to only account for only the minimum distance nonbonded interactions between atoms i and j, and not between all images. This minimum distance interaction may occur between atoms i and j located either in the central box or between atom i in the central box and atom j in an image. CHARMM reduces computational costs of cubic PBC by considering only images to the right, top, and behind of the central box, as well as the relevant edge and vertices images, reducing the

total number of images to 14. Also for large systems, only atoms within the cut-off radius are replicated.

1.2.5 Integration

In CHARMM the leap frog verlet (Eqs. 1-3 & 1-4) was used where position, $\vec{r}$, and velocity, $\vec{v}$, of the atoms were calculated at interleaved time points, $t \pm 1/2$, with a time step size of δt. The velocity at the next half step in time is first calculated, and then subsequently used to calculate the position at the next point time.

$$\vec{v}_{t+1/2} = \vec{v}_{t-1/2} + \vec{a}_t \delta t \tag{1-3}$$

$$\vec{r}_{t+1} = \vec{r}_t + \vec{v}_{t+1/2} \delta t \tag{1-4}$$

The NAMD, the velocity verlet algorithm is used. The position at the next point in time is calculated from the velocity and acceleration at the same point in time as follows.

$$\vec{r}_{t+1} = \vec{r}_t + \vec{v}_t + \vec{a}_t \delta t^2 \tag{1-5}$$

$$\vec{v}_{t+1/2} = \vec{v}_t + \frac{1}{2}\vec{a}_t \delta t \tag{1-6}$$

$$\vec{a}_{t+1} = \frac{-1}{m} \nabla U(\vec{r}_{t+1}) \tag{1-7}$$

$$\vec{v}_{t+1} = \vec{v}_{t+1} + \frac{1}{2}\vec{a}_{t+1} \delta t \tag{1-8}$$

1.2.6 Temperature and Pressure Control

In CHARMM a Hoover thermostat (Hoover 1985) was used to control temperature. In this extended system approach a temperature bath is included with the system which adds an extra degree of freedom, s. The potential energy of the temperature bath is given by

$(f+1)k_BT\ln s$ where f is the degree of freedoms in the physical system, k_B is the Boltzmann constant, and T is the desired temperature. The kinetic energy of the temperature bath is given by $(Q/2)(ds/dt)^2$ where Q is considered to be the mass, and has units of energy times time^2. Energy is exchanged slower as Q increases.

In NAMD, temperature was held near a constant value, T, by using Langevin dynamics. The equations of motion were modified so that the particles were subject to partial damping by including collision and random force terms where γ is the collision frequency and $\eta(t)$ is a force following a Gaussian probability distribution with mean = 0 and variance $2\gamma k_B T\delta(t)/m_i^{-1}$ where $\delta(t)$ is the dirac delta function.

$$\frac{d^2\vec{R}_i}{dt^2} = -\frac{1}{m_i}\nabla U_i - \gamma\frac{d\vec{R}_i}{dt} + \eta(t)\sqrt{2\gamma k_B T m_i^{-1}} \qquad (1\text{-}9)$$

To control the pressure in MD simulations, the central box size is allowed to change isotropically. In CHARMM, pressure was controlled with the Nosé-Hoover piston (Nosé 1983), which is similar to the Hoover thermostat. In this extended system approach an extra degree of freedom, V, corresponding to the volume was added to the system. The potential energy of the system is PV, where P is the desired pressure. The kinetic energy of extended system is $(Q/2)(dV/dt)^2$where Q is the mass of the piston of units mass times length^{-4}.

In NAMD, a Langevin piston (Feller et al. 1995) was used to control the pressure. The extended system approach is used again, but the piston is subject to partial damping by a collision term and random force (from a Gaussian distribution with mean = 0 and variance $2\gamma k_B T\delta(t)/Q$) term. The piston temperature was coupled to a temperature bath through Langevin dynamics.

CHAPTER 2 COMPOSITION OF TOP6 *E. COLI* MEMBRANE

2.1 Introduction

There are three important quantities to consider when defining the cytoplasmic membrane composition of *E. coli*. The most obvious quantity is the ratio of specific lipids which consist of a hydrophilic head group and acyl-chains. The ratio of phosphoethanolamine (PE): phosphoglycero (PG) lipids is another important quantity. It has been well established that the *E. coli* membrane is composed of mostly PE lipids and some PG lipids. PG lipids are important because they stabilize bacterial membranes (Zhao et al. 2007) and are essential for certain crucial proteins such antimicrobial peptides (AMPs) (Cirac et al. 2011). Lastly, the relatively minor amount of cardiolipin present in the membrane should be characterized to determine if this lipid is important in developing an accurate membrane model. Cardiolipin is a diphosphatidylglycerol, which is important for the structure and function of large membrane enzymes, especially those involved in energy metabolism (McAuley et al. 1999).

There have been an extensive amount of studies using various techniques that measure the *E. coli* membrane composition, which include compositions of the inner and outer membrane, of different strains, and during various growth stages (Shokri and Larsson 2004). Furthermore, the effects of temperature (Morein et al. 1996), chemicals (Dombek and Ingram 1984; Ingram 1977), nutrients (Razin 1975; Letellier, Moudden, and Shechter 1977), pH, and genetic modifications have been investigated (Letellier, Moudden, and Shechter 1977). In general, all of these factors affect the composition to varying degrees. Thus, the reported compositions of the cytoplasmic *E. coli* membrane can differ greatly. For example, reported

PE:PG vary from 3:1 to 7:1. Cardiolipin has been measured to make up anywhere from 1 – 10 % of an *E. coli* membrane. C16:0 is generally observed as a well populated FA, but C18:1 ranges from 10 – 30% of the total membrane FA composition, and cyclic FAs are sometime not reported at all.

2.2 Methods

It would have been incorrect to develop a comprehensive *E. coli* membrane composition based on data obtained from a wide parameter space, so an intuitive search criterion was implemented. The first criterion focused the search towards K12 strains because the strain and its derivatives are widely used in research and industry (US EPA). Secondly, studies investigating the effects of genetic modification or chemicals were discarded, because of observed unnatural artifacts in the membrane composition. A third criterion narrowed the literature to *E. coli* grown only on standard Luria Broth (LB), again because of its wide use.

A combination of two independent studies was used to define the lipid composition of the complex membrane referred to in this thesis as Top6. In one study, the relative composition of lipid mass:charge (m/z) ratios of a LM 3118 K12 *E. coli* was found using a high pressure liquid chromatography/electrospray ionization tandem mass spectrometry technique (LC/MS/MS) (Oursel et al. 2007). Cultures were grown in LB at pH 6.95 and 37 °C overnight before harvesting. The analysis identified 13 PG and 17 PE lipids taking into account isobaric forms. Isobaric forms were m/z species which could be explained by different combinations of FA chains at the *sn*-1 or *sn*-2 position.

In the second study, the FA composition of NBRC 3301 K12 *E. coli* was determined using two different but complementary analyses; thermally assisted hydrolysis and methylation-

gas chromatography (THM-GC) and conventional gas chromatography (GC) (Ishida et al. 2006). Cells were cultured on LB agar at 37 °C for 24 hours. The analysis identified 9 different FAs ranging from 14 to 19 carbons in length. The FA composition data from this study was used to estimate the fraction of each FA combination in isobaric forms from the LC/MS/MS study's m/z population.

The data sets from the two studies were combined to create the composition of the complex membrane. First, both data sets were slightly conditioned. Only the 6 most abundant m/z species (top 6), including the isobaric forms of some m/z species, from the LC/MS/MS study were chosen. A fatty acid distribution was derived from the relative composition of the species. The second FA distribution was averaged from the THM-GC and GC analyses and FAs which were absent from the chosen top 6 m/z species were ignored. To adjust for the absent FAs, the remaining portion of the distribution was reallocated between the two most popular FAs. This adjusted distribution was the target FA distribution.

Major isobaric forms in the top 6 m/z species were identified by minimizing the sum of square errors between the two FA distributions with constraints. The constraints allowed the relative composition of the top 6 m/z species vary between the reported errors. Also, the isobaric fraction of a m/z species was allowed to vary between 0 and 1, but all fractions of a m/z species were constrained to sum to 1 (Fig. 2.1). The minimization was run several times with different initial conditions. Obsolete isobaric forms were ignored, and the actual simulated *E. coli* membrane composition was determined by a guess and check method so that the error with the target composition was minimized. It was also ensured the total number of lipids would form a bilayer of a suitable size for a MD simulation.

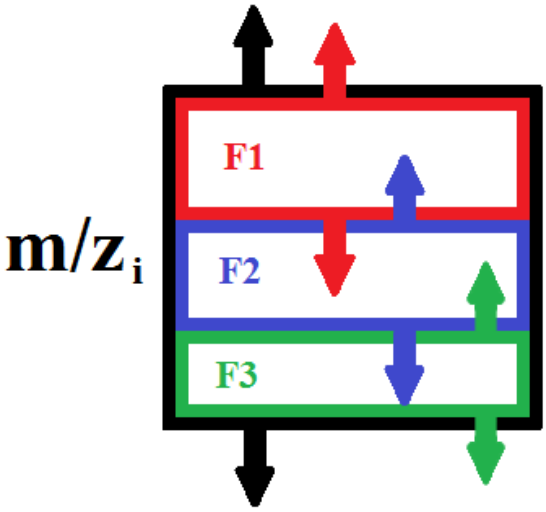

Figure 2.1 Constraints on relative m/z species compositions and fractions of isobaric forms. The relative composition of m/z species i was allowed to vary between the reported standard deviation**,** represented by black box and arrows. The isobaric fractions, represented by colored boxes, were allowed to vary between 0 and 1, but the sum of isobaric fractions for a given m/z species was constrained to 1.

2.3 Results

Oursel et al. identified 20 separate m/z species from their *E. coli* samples. We chose the top 6, as shown in Figure 2.2, which constituted about 70% of all the m/z species. The corresponding lipid/isobaric forms to their m/z species are listed in Table 2.1.

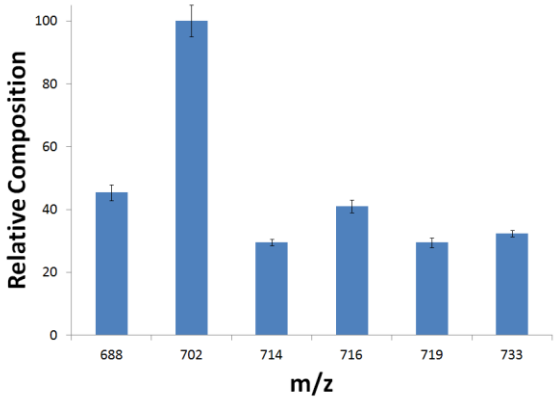

Figure 2.2 Relative composition of 6 most abundant m/z species. 702, 716, and 733 were identified as specific lipids. 688, 714, and 719 were identified with two or more possible isobaric forms. Data taken from **(Oursel et al. 2007)**.

The conditioning of the fatty acid distribution from the THM-GC and GC analyses, is listed in Table 2.2. The first two rows contain the unconditioned data from the two different techniques. The third row contains the averages of the FAs which were found in the top 6 m/z

species (Table 2.1), with the exception of C14:0 because it was later found to be insignificant. The last row contains the FA distribution adjusted for the ignored FAs.

m/z	*sn*-3 *sn*-2/*sn*-1	Fraction
688	PE C15:0/cyC17:0	0.13
	PE C16:0/C16:1	0.04
702	PE C16:0/cyC17:0	0.43
714	PE C18:1/C16:1	0.07
	PE cyC17:0/cyC17:0	0.00
716	PE C16:0/C18:1	0.12
719	PG C14:0/C18:1	0.00
	PG C15:0/cyC17:0	0.00
	PG C16:0/C16:1	0.12
733	PG C16:0/cyC17:0	0.09

Table 2.1 Corresponding lipids/isobaric forms to m/z species and composition after error minimization.

	C14:0	C15:0	C16:0	C16:1	C17:0	cyC17:0	C18:0	C18:1	cyC19:0
THM-GC‡	9.0	12.9	32.1	8.9	3.5	21.7	2.7	5.2	4.0
GC‡	4.0	12.2	36.7	9.4	3.5	21.9	4.1	5.3	2.9
Avg.§§	–§	12.5	34.4	9.2	–	21.8	–	5.3	–
Adj.	–	12.5	48.1	9.2	–	31.0	–	5.3	–

Table 2.2 Conditioning of FA distribution from THM-GC and GC analysis.
‡ Data taken from **(Ishida et al. 2006)**.
§ C14:0 was found in an isobaric form of one m/z species, but later found to be insignificant.
§§ Fatty acids absent from m/z species ignored.

Minimization of the sum of square errors between the FA distribution from the LC/MS/MS and THM-GC/GC studies isolated one major form in the top 6 m/z species with multiple isobaric forms (See Table 2.1). The obsolete isobaric forms were ignored and the top 6 m/z species were narrowed to 6 specific lipids. The composition of the lipids was held constant to the minimized m/z species composition, while the integer number of lipids was scaled up. For a suitable size MD simulation, about 75 lipids per leaflet were needed. The total number of lipids per leaflet which matched the target FA composition closest, and was a good size as determined by guess and check was 78 lipids.

The simulated composition of the complex *E. coli* membrane, referred to as Top6, is shown in Figure 2.3 (next page). The final PE:PG was 4:1 (Fig. 2.3 A). The two major FAs, accounting for 75 % of all FAs, were cyC17:0 and C16:0 (Fig. 2.3 B). The dominant lipid, making up nearly half of the membrane was 1-palmitoyl-2-*cis*-9,10-methylene-hexadecanoic-acid-glycero-3-phosphoethanolamine (Fig. 2.3 C), which we abbreviate as PMPE where M contains the cyclic moiety. Other lipids included were POPE and the PG analog of PMPE, 1-palmitoyl-2-*cis*-9,10-methylene-hexadecanoic-acid-glycero-3-phosphoglycerol (PMPG). Structures of all the lipids are shown in Figure A.1 (Appendix). Noticeably absent were POPG, which was used in previous model *E. coli* membranes, and cardiolipin. Since cardiolipin was only found in small amounts it was neglected. However, it has been observed that cardiolipin localizes in septal and polar regions of *E. coli* (Mileykovskaya and Dowhan 2000). Therefore, the Top6 membrane is not apt for these regions of the *E. coli* membrane, and an appropriate number of cardiolipins should be added.

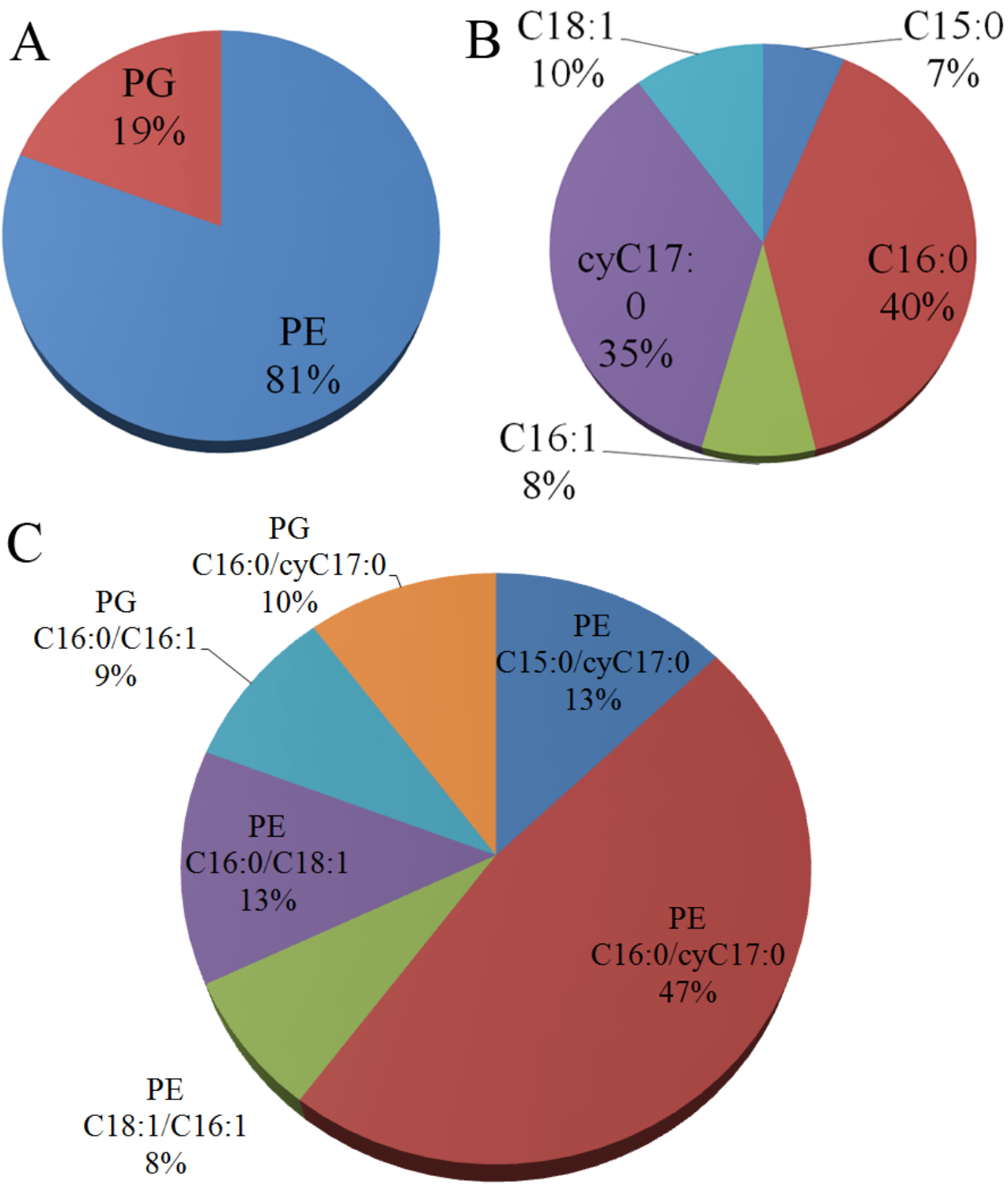

Figure 2.3 Final Top6 composition. (A) Top6 PE:PG. (B) Top6 FA composition. (C) Top6 lipid composition.

CHAPTER 3 PARAMETERIZATION OF CYCLIC MOIETY

3.1 Introduction

Lipids with cyclic moieties in the fatty acid chain had never been simulated before with a CHARMM FF. Therefore, parameters consistent with the CHARMM FF needed to be developed to describe the cyclopropane ring. Parameterization of additions to an existing FF is a non-trivial task. Experimental data of structural or thermodynamic properties should be selected to help guide parameterization. *Ab initio* quantum mechanics (QM) calculations may also be used to guide parameterization in the absence or lack of experimental data. Focus is placed towards nonbonded and dihedral parameters because FF performance is more sensitive to their changes than of angle bending or bond stretching terms (Leach 2001).

Parameterization of the cyclic moiety in PMPE began by searching the C36 General FF (Vanommeslaeghe et al. 2010) for suitable parameters. In this case, parameters from cyclopropane and similar molecules for Lennard-Jones, electrostatic, bond, and angle terms were found. Additionally, *cis* double bond dihedral parameters from the C36 Lipids FF were used to describe the acyl backbone portion of the ring (dihedrals θ_1=9-10-11-12 and θ_2=10-11-12-13). However, this produced results which were in disagreement with experimental deuterium order parameters (S_{CD}) profiles of a nearly identical lipid.

S_{CD} profiles are calculated from ^{2}H NMR spectra and measures the C-H vector order with respect to the bilayer normal. Therefore it provides structural information and can be used to track phase changes. As the order parameter increases the chain order increases as well. Broadly speaking, the order parameter is expected to decrease down the acyl chain.

We hypothesized that the *cis* double bond dihedral parameters were inadequate for the cyclic moiety. Thus, the ring dihedrals were subsequently reparameterized by fitting them to high-level QM calculations.

3.2 Methods

As stated earlier, the C36 Lipid and General FF were searched through to find similar atoms, bonds, and angles. Nonbonded, bond, angle, and dihedral parameters for only the cyclic moiety (C9, C10, C17) were found from parameters for cyclopropane in the C36 General FF. Bond and angle parameters with neighboring carbons were found from larger molecules with a cyclopropane ring. The full cyclic moiety FF can be found in the Appendix.

To fit the dihedrals, first the potential energy surface of small model compounds without any dihedral terms for θ_1 and θ_2 was calculated (Fig. 3.1). The dihedral angle was fixed at 1° intervals from 0° to 360°. At each interval the potential energy of the structure was minimized structure in CHARMM by the steepest descent (SD) and adopted base Newton-Raphson (ABNR) method. The SD method uses only the first derivative of the potential to move the atoms in the same direction as the net force. The ABNR method employs SD as well and applies the Newton-Raphson scheme, which uses the first and second derivatives, to only a subspace of the molecule.

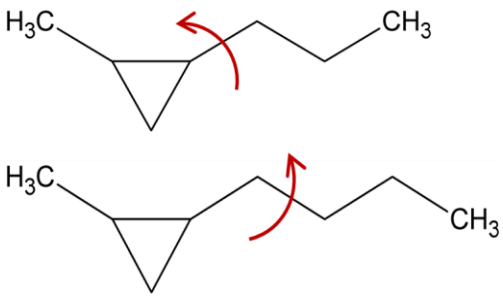

Figure 3.1 Model parameterization compounds. The model compounds used for potential energy surface calculations for θ_1 and θ_2 (top and bottom, respectively).

High-level QM calculations were done using the Gaussian03 suite of programs (Frisch et al. 2003). The previously developed hybrid method (HM-IE) (Klauda et al. 2003) was used to estimate the conformational energies at the CCSD(T)/cc-pVDZ in vacuum. The two dihedrals were scanned at 15° intervals using the two model compounds.

The dihedral potential energy term is described by a set of cosine terms, as shown in Eq. 3-1, where multiple minimum dihedral angles, φ, can exist. For each cosine term, j, the relevant FF parameters are the dihedral force constant, K_φ, multiplicity (number of minimums), n, and phase angle, δ.

$$U_{dihedral}(\vec{R}) = \sum_{dihedrals} \sum_{j} K_{\varphi,j}\left(1 + \cos\left(n_j\varphi - \delta_j\right)\right) \qquad (3\text{-}1)$$

The dihedral potential was fit to the target data, the difference between the QM and CHARMM determined potential surfaces, using a general conformational-energy fitting procedure developed by Guvench & MacKerrel (Olgun Guvench and MacKerell 2008). The procedure is based on a Monte Carlo simulated annealing process which minimizes the root mean square deviation between the target energy and parameterized energy. The target data was weighted using a Boltzmann distribution. The procedure was run several times to confirm convergence.

A pure PMPE bilayer was constructed with the aid of CHAMMM-GUI (Jo et al. 2008). It consisted of 71 lipids per leaflet and hydrated with 31.8 waters per lipid. The total system size was 32,223 atoms. Missing coordinates were generated in CHARMM (B R Brooks et al. 2009). CHARMM-GUI scripts for minimization and equilibration of bilayers were also carried out in CHARMM. Care was taken to restrain *cis* double bonds and *cis* cyclopropane rings during

minimization. A short 21 ns simulation was also run with the previous version C36c with double bond dihedral parameters for the ring moiety. However care was not taken to restrain *cis* double bonds and *cis* rings during minimization, which caused some lipids to switch to the *trans* conformation.

NAMD (J. C. Phillips et al. 2005) was used to perform isothermal-isobaric ensemble (NPT) simulations of the bilayer. All simulations were performed under the following protocol. A Lennard-Jones force-based switching function over 8 to 12 Å was implemented. Particle Mesh Ewald (Darden, York, and Pedersen 1993) was used for long-range electrostatics. Membranes were simulated for 50 ns with 2 fs time steps. Hydrogen atoms were constrained using the SHAKE (Ryckaert, Ciccotti, and Berendsen 1977) algorithm. The temperature and pressure were held at 310.15 K and 1 bar, respectively. Temperature and pressure control was achieved through Langevin dynamics and a Langevin Piston (Feller et al. 1995). The membrane was simulated 3 times using the cyclic modified CHARMM36 (C36c) FF.

The surface area per lipid (box length squared divided by number of lipids per leaflet), SA, was tracked to monitor whether the simulation was in equilibrium. The S_{CD} of each C-H vector was calculated as follows

$$S_{CD} = \left|\left\langle \frac{3}{2}\cos^2\beta - \frac{1}{2}\right\rangle\right| \tag{3-2}$$

where β was the angle between the C-H vector and bilayer normal. Experimentally, the order of C-^{2}H vectors are determined by measuring the quadrupolar splitting between the peaks of the powder spectrum (Fig. 3.2) and calculating the S_{CD} as follows

$$S_{CD} = \frac{4}{3}\Delta\nu_Q / A_Q \tag{3-3}$$

where $\Delta\nu_Q$ was the quadrupolar splitting and $A_Q$was the quadrupolar coupling constant.

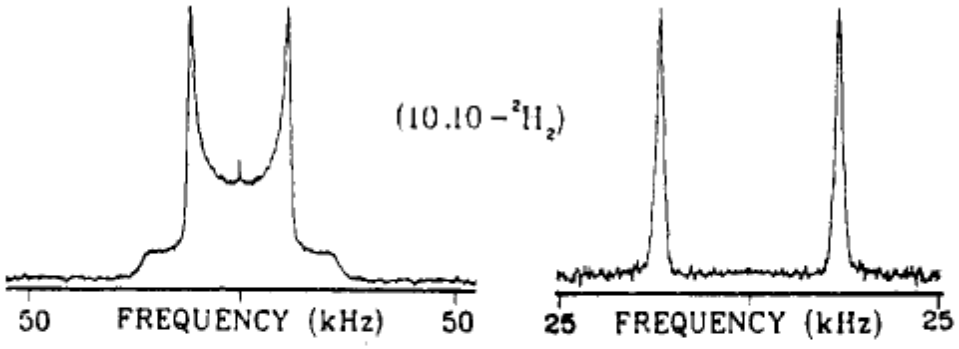

Figure 3.2 Example NMR spectra. Experimental powder (*left*) and depaked (*right*) ^{2}H NMR spectra at the 10 carbon position in an acyl chain with a cyclopropane ring moiety. Figure taken from **(Dufourc, Smith, and Jarrell 1984)**.

3.3 Results

The potential energy surface of the two parameterized dihedrals is shown in Figure 3.3. The C36c FF matches the dihedral profile as calculated from QM and is superior to the C36 FF profile with its double bond parameters. Each fitted dihedral consisted of a set of 3 cosine terms which are listed in Table 3.1.

Dihedral	K_χ	n	δ
9-10-11-12	1.71	1	159.6
	0.37	2	165.1
	0.58	3	47.6
10-11-12-13	0.16	1	180.0
	0.01	2	180.0
	0.17	3	180.0

Table 3.1 Dihedral parameters for cyclic moiety.

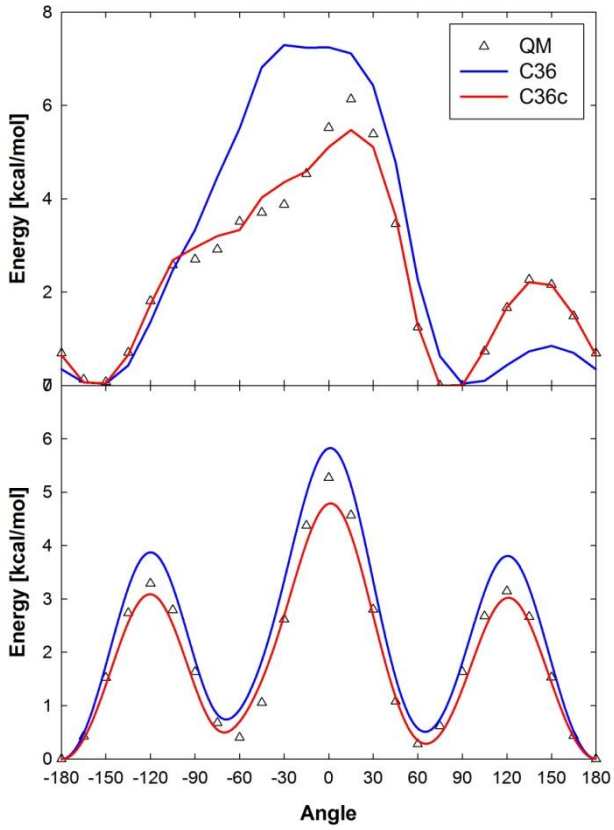

Figure 3.3 Dihedral profiles for θ_1 (*top*) and θ_2 (*bottom*).

Once the dihedral parameters were in good agreement with the QM calculations we performed MD simulations of a fully hydrated PMPE bilayer. The first step was to equilibrate the bilayer which took about 5 ns of MD simulation time after minimization. The equilibrium was monitored by the calculating the surface area per lipid, which was fairly constant at around 63 ± 1 Å (See Fig. A.1).

To evaluate how well the ring moiety was parameterized in the cyclic lipids, we compared the calculated S_{CD} profile of PMPE from the MD trajectories with experiment. The quadrupolar splitting of a PE cy19:0/16:0 (PDSPE) lipid (at *sn*-2 carbon 5, 9, 10, & 16 positions) at 40^o C (Bruno Perly, Smith, and Jarrell 1985) and PC cy19:0/16:0 (PDSPC) lipid (at *sn*-2 carbon 2, 5, 8-11, 16, & 19 positions) at 40^{o}C (Dufourc, Smith, and Jarrell 1983) were measured experimentally (Fig. 3.4). The effect of the longer *sn-2* acyl change was assumed to be

negligible. The numbering and structures of PMPE, PDSPE, and PDSPC are shown in Figure 3.4.

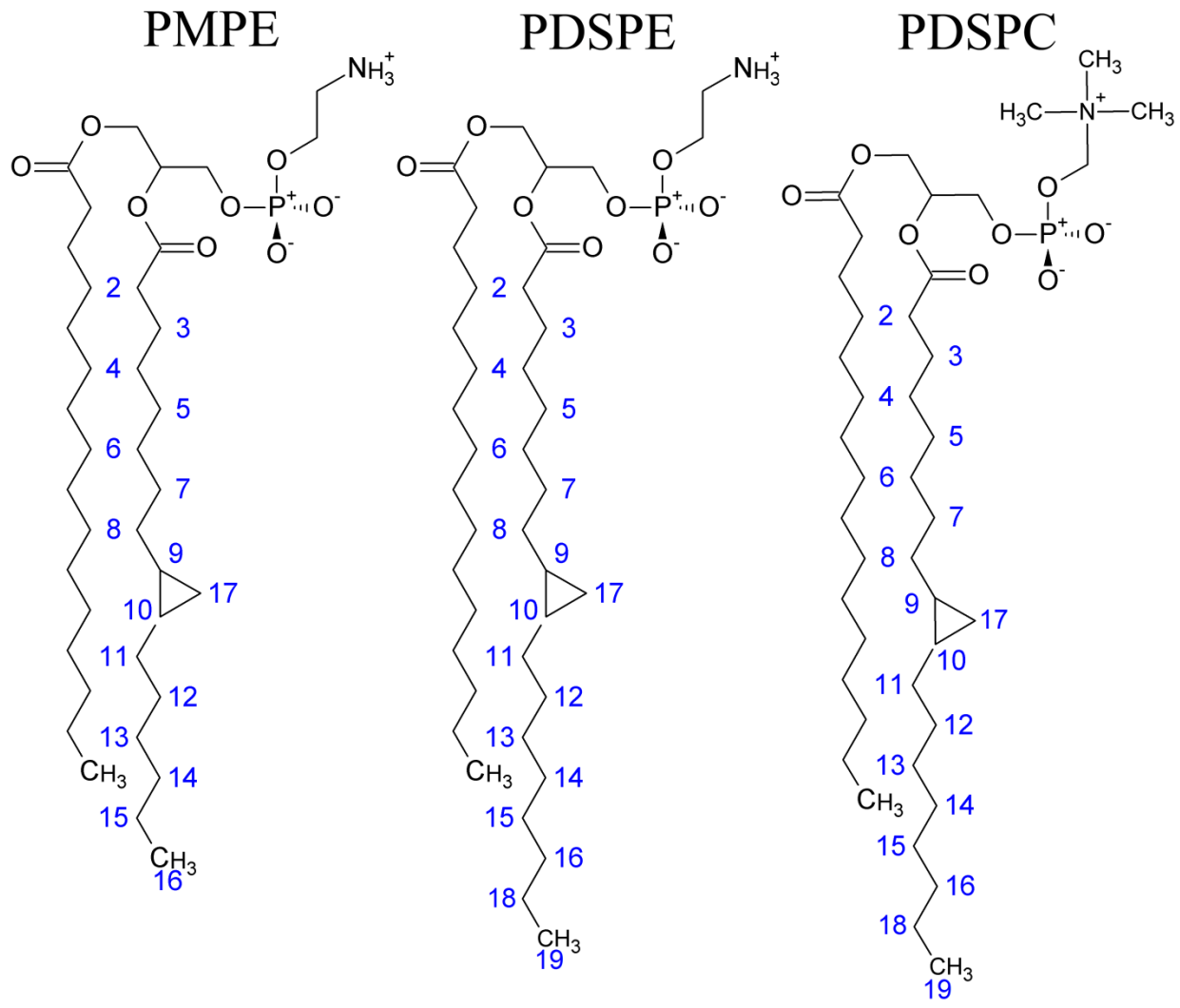

Figure 3.4 Structures and numbering of PMPE, PDSPE, and PDSPC. The ring carbon in PDSPE and PDSPC is numbered 17 for consistency.

Our initial attempts to describe the cyclic moiety with double bond parameters led to an incorrect S_{CD} profile (Fig. 3.5, next page). The S_{CD}s of PMPE with double bond ring parameters were calculated from only *cis* PMPE, but the simulation contained both *cis* and *trans* PMPE due to an error during minimization. Splitting at C8 and C17 is consistent with experiment; however the relative order to neighboring carbons is wrong. For example C17 is supposed to be more ordered than C9 and C10.

Reparameterizing the ring dihedrals produced an S_{CD} profile which matched the experimental data better (Fig. 3.5, next page). The S_{CD}s from the cy19 PE lipid matched very well with our calculated parameters for C5 and C9. Conversely, we underestimate the C10 order by 0.04. Still, we matched the trend that C10 is more disordered than the C9. The S_{CD}s at the 16 position did not match because PMPE consists of a terminating methyl group at that position where as the cy19 PE lipid consists of a methylene group.

Comparing the S_{CD}s of the cy19 PC lipid to cy19 PE lipid, we noticed the cy19 PC parameters were shifted down. We concluded that the S_{CD}s from the PC lipid would underestimate the order profile of the PMPE, but general patterns would be consistent, specifically the existence of S_{CD} splitting at C8, C17, and C11. Our calculated S_{CD}s at these positions did not show statistical splitting, but did match with at least one of the C-H vectors. Taking into account a larger head group and longer acyl chain, we feel our S_{CD} profile of PMPE with the C36c FF matches the pattern observed from experiment.

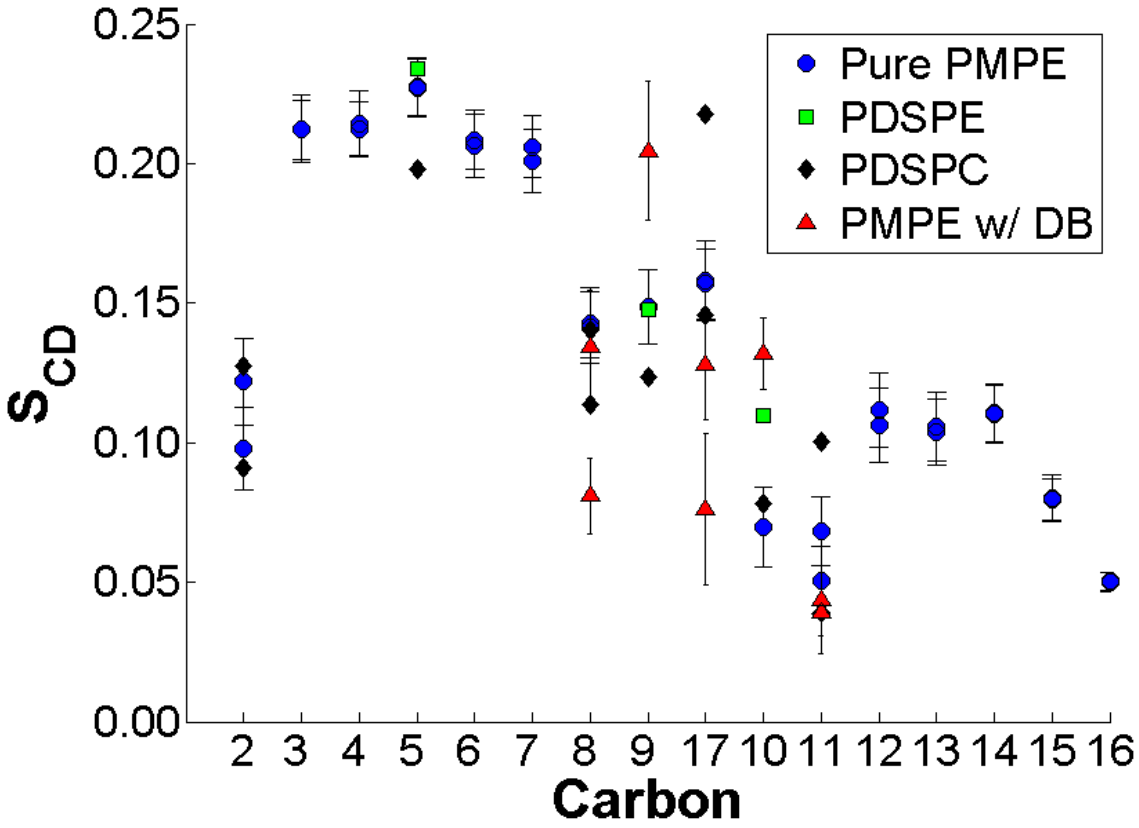

Figure 3.5 PMPE S_{CD} profile. S_{CD} of *sn*-2 chain of PMPE in a pure PMPE membrane with the C36c FF (*blue circles*), PDSPE from experiment at 40 °C (Dufourc, Smith, and Jarrell 1983) (*green squares*), PDSPC from experiment at 40 °C (Bruno Perly, Smith, and Jarrell 1985) (*black diamonds*), and PMPE in a pure PMPE membrane with double bond parameters (*red triangles*). The S_{CD} of PDSPE and PDSPC were calculated using equation 2 based on quadrupolar splitting data and A_Q= 170 kHz (Burnett 1971) and 183 kHz (Dufourc, Smith, and Jarrell 1983) for sp3 hybridized (including C17) and cyclopropane (C9 and C10) carbons respectively.

It is also worthy to note that Dufourc measured the effect of the cyclopropane ring on the phase transition from a bilayer to a hexagonal phase. In PE lipids, it reduces the transition temperature from between 55 and 75 ^{o} C to 38 and 58 ^{o} C (Dufourc, Smith, and Jarrell 1983). According to Dufourc (Dufourc, Smith, and Jarrell 1983), at 40^{o} C, nearly all of the cyclic lipid

system was in the bilayer phase. Also, we would like to enforce that no evidence of a phase transition during our short simulations was observed.

CHAPTER 4 COMPLEX *E. COLI* MEMBRANE

4.1 Introduction

Simple model *E. coli* membranes have been developed before. However, the question as to if the simplification of the membrane is sufficient or not, has not been answered. Part of the reasoning for no validation, is that experimental data from intact cells or natural membranes of important properties such as the membrane thickness is difficult to measure. Also, the primary use of model membranes is not to study the lipids, but to study integral and peripheral membrane proteins. Properties of the membrane such as the thickness (Kim and Im 2010), surface density, and compressibility (Wiggins and Phillips 2005) will affect protein behavior and structure. Thus, the quality of the model membrane may be assessed by its interaction with proteins.

The goal of this study was to develop an accurate representation of an *E. coli* cytoplasmic membrane for use in further simulation studies. It has routinely been found that bacterial membranes are mainly composed of phosphoethanolamine (PE) and phosphoglycerol (PG) lipids. Murzyn et al. (Murzyn and Pasenkiewicz-Gierula 1999) previously developed an *E. coli* computer model membrane with a 3:1 POPE:POPG lipid bilayer. Zhao et al. (Zhao et al. 2007) also developed a 3:1 POPE:POPG membrane to study the role of PG lipids in stabilizing bacterial membranes. An important constituent of several bacterial membranes are lipids with a cyclic moiety (Dufourc, Smith, and Jarrell 1984; Grogan and Cronan 1997), which have been neglected in previous works. A model *E. coli* membrane consisting of saturated, unsaturated, and

cyclic-containing lipids was simulated along with a standard POPE/POPG model for comparison. Deuterium order parameter (S_{CD}) profiles were calculated, which differentiates cyclic lipids from monounsaturated lipids. The thickness of the membranes was measured from their respective electron density profiles (EDP). Finally, the surface area per lipid and area compressibility modulus was calculated to evaluate bulk properties of the membranes.

4.2 Methods

Coordinates for all membranes were taken from membranes developed through CHARMM-GUI (Jo et al. 2008) (see Table 4.1 for details). Missing coordinates were generated in CHARMM (B R Brooks et al. 2009). CHARMM-GUI scripts for minimization and equilibration of bilayers were also carried out in CHARMM. Care was taken to restrain *cis* double bonds and *cis* cyclopropane rings during minimization.

Membrane	PE:PG	Water:Lipid	Total Lipids	Total Atoms
POPE/POPG	5.3:1	32.7	152	32222
Top6	4.2:1	32.8	156	33134

Table 4.1 Compositions of model membranes.

NAMD (J. C. Phillips et al. 2005) and CHARMM programs were used to perform isothermal-isobaric ensemble (NPT) simulations of the bilayers. All simulations were performed under the following protocol. A Lennard-Jones force-based switching function over 8 to 12 Å was implemented. Particle Mesh Ewald (Darden, York, and Pedersen 1993) was used for long-range electrostatics. Membranes were simulated for 50 ns with 2 fs time steps. Hydrogen atoms were constrained using the SHAKE (Ryckaert, Ciccotti, and Berendsen 1977) algorithm. The temperature and pressure were held at 310.15 K and 1 bar, respectively. In the CHARMM simulation, temperature and pressure control was achieved with a Hoover thermostat (Hoover

1985) and Nosé-Hoover piston respectively (Nosé 1983). In NAMD simulations, temperature and pressure control was achieved through a Langevin Piston (Feller et al. 1995) coupled with the temperature of the piston coupled to Langevin dynamics. Each membrane composition was simulated 3 times using the cyclic modified CHARMM36 force field (C36c) (Klauda et al. 2010).

Upon completion of the simulations the trajectories were analyzed to compute overall surface areas per lipid, deuterium order parameters, electron density profiles, compressibility moduli, and compression energy density. The surface area per lipid (lateral box length squared divided by number of lipids per leaflet), SA, gave a general idea of the packing of the lipids within the membrane plane. It was also tracked to monitor whether the simulation was in equilibrium. The deuterium order parameters (S_{CD}) of the acyl chains were calculated as per Equation 3-2. The electron density profile (EDP) was calculated using a binned method along the bilayer normal. The thickness of the membrane, *Z*, was calculated as the peak–to–peak distance of the total EDP in each leaflet. The hydrophobic core thickness, *D*, was measured as the peak–to–peak distance of the carbonyl EDP in each leaflet. The compressibility modulus is a measure of the stiffness of the membrane and was calculated as,

$$K_A = k_B\langle T \cdot A\rangle/\sigma_A^2 \tag{4-1}$$

where k_B was the Boltzmann constant, T was the temperature, A was the area, and σ_A^2 was the variance of the area during the simulation. The compression energy density (CED) of the bilayer illustrates the amount of energy necessary to compress or expand the membrane and was defined as,

$$CED = \frac{1}{2}K_A(d - d_0/d_0)^2 \tag{4-2}$$

where d was the thickness of the perturbed bilayer, and d_0 was the average bilayer thickness.

4.3 Results

During the course of all the simulations, the surface area per lipid remained fairly constant (See Fig. A.2). The Top6 membrane had a surface area per lipid of and 64 ± 1 $Å^2$. The POPE/POPG membrane was slightly denser with a surface area per lipids of 60 ± 1 $Å^2$ per lipid.

Double bonds are well known to induce local disordering as observed in the order profile of POPE (Fig. 4.1, next page). Before the double bond, the average order parameter of C3-C7 was 0.21. A sharp decrease in the order parameter to an average of 0.075 is seen at the double bond, C9 and C10. The effect of the double bond is also seen in its adjacent carbons, C8 and C11 where the average order parameter is 0.1. The general order profile of PMPE was similar to POPE but there were notable differences in the ring region. The average order parameter of C3-C7 before the ring was 0.21 and C10 in the ring was 0.075, both similar to POPE. However, the order parameter of C9 in the ring was 0.15 and the adjacent carbons of the ring (C8 and C11) were similarly disordered as their neighboring ring carbons, a marked contrast from POPE. Also, the branched carbon of the ring C17 was of equal order as C9. The S_{CD} profiles of the other lipids in the Top6 membrane, shown in the Appendix (Fig. A.2), followed the previously observed trends of cyclic, double bond, and saturated moieties.

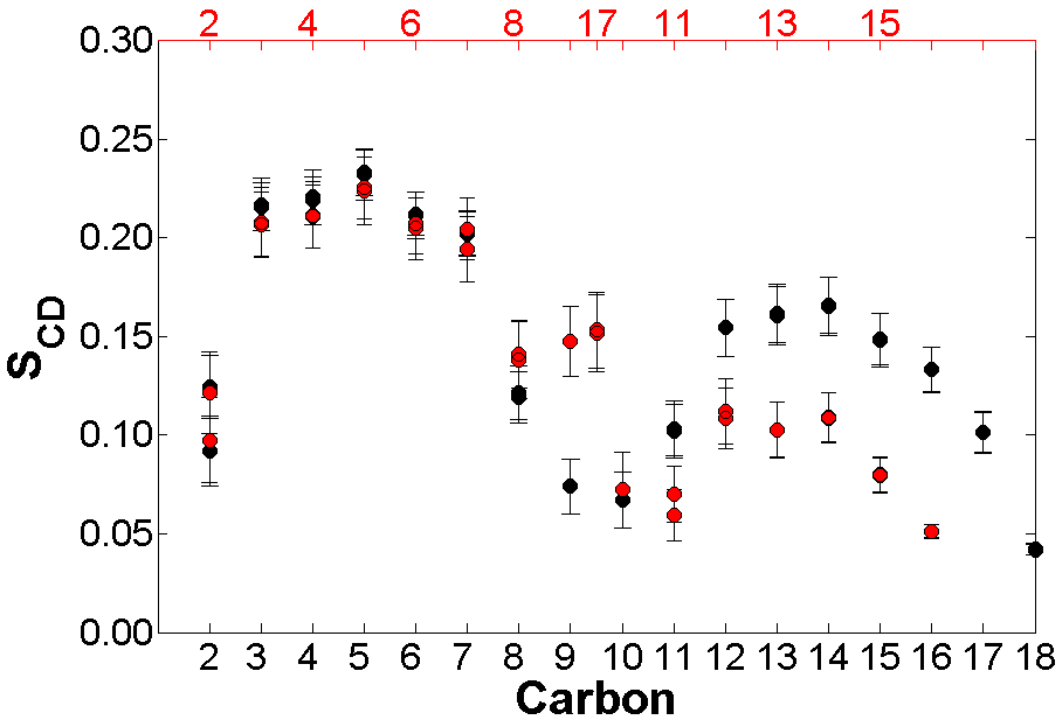

Figure 4.1 PMPE and POPE S_{CD} profile. S_{CD} of *sn*-2 chain of PMPE in the Top6 membrane (*red*) and of POPE in the POPE/POPG membrane (*black*).

Overall the EDPs of the membranes had the same general shape. The profile consisted of the density of bulk water (z > 30 Å), the phospholipid head groups (z ~ 17-21 Å), the carbonyls (z ~ 17-21 Å), the double bonds and rings (z~5-10 Å), and the tail ends of the lipids (z~0) (Fig. 4.2). Component density peak location and distribution width as fitted by Gaussians are listed in Table 4.2. The peak–to–peak distances indicate the Top6 membrane is slightly thinner than the POPE/POPG membrane. The thickness, *Z*, of the Top6 membrane was 37.3 ± 0.2 Å while the POPE/POPG membrane was 40.1 ± 0.1 Å. The hydrophobic core thickness, *D*, of the Top6 and POPE/POPG membranes were 29.8 ± 0.1 and 32.7 ± 0.3 Å respectively. The POPE/POPG membrane was thicker than the Top6 membrane due to the longer lipids.

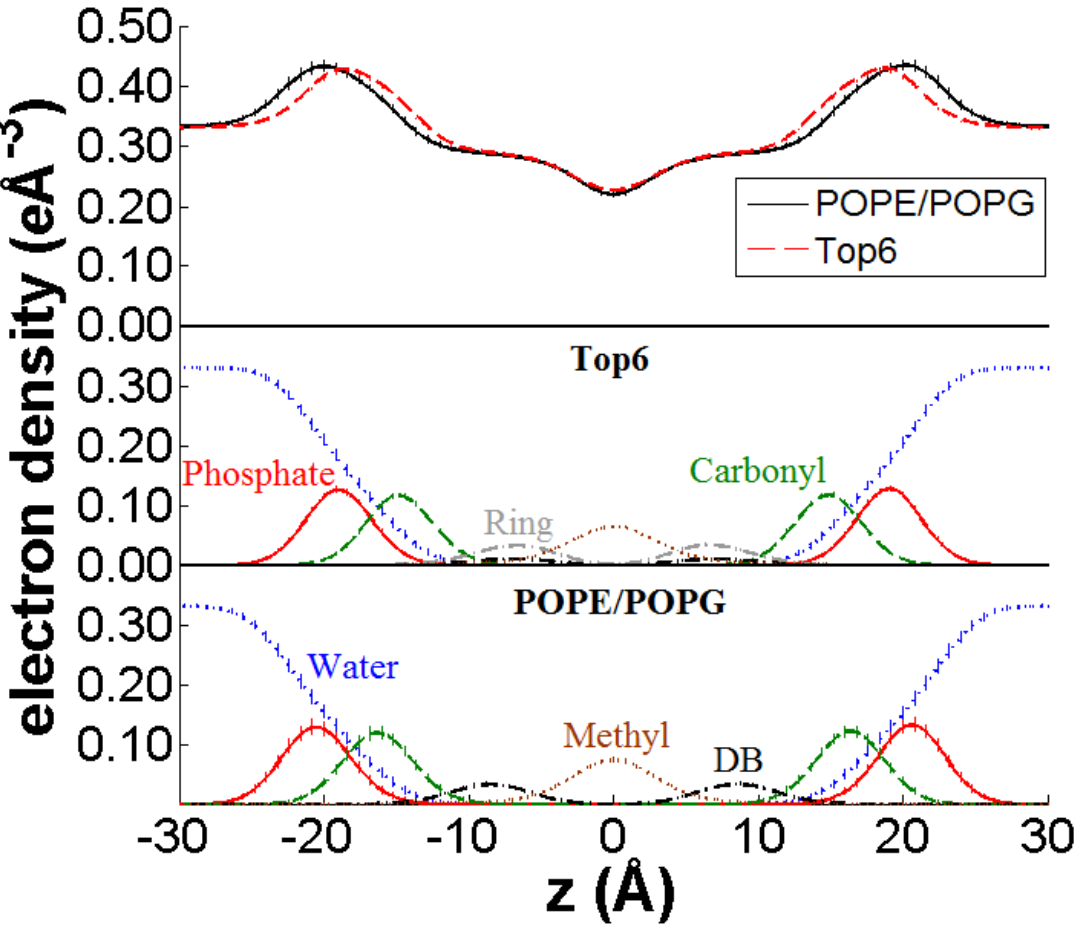

Figure 4.2 Electron density profiles. Total electron densities (*top*), Top6 component densities (*middle*) and POPE/POPG component densities (*bottom*). The Top6 membrane is thinner than the POPE/POPG membrane. Water (*dotted blue*), phosphate (*solid red*), carbonyl (*dashed green*), ring (*dash dotted grey*), double bond (DB) (*dash dotted black*), and methyl (*dotted brown*) component EDP curves are labeled and are the same for both middle and bottom panels.

The length of the hydrophobic region of each lipid in the Top6 membrane was surprisingly similar given the varying lengths of the acyl chains. Thus, the longer lipids were either compressing or interdigitizing. The hydrophobic chain thickness of POPE in the POPE/POPG membrane was 32.7 ± 0.3 Å, but in the Top6 membrane it was 29.9 ± 0.6 Å. However the distance between C2 and C18 atoms in POPE in both the POPE/POPG and Top6 membranes was the same, about 16 Å, indicating the lipids were not compressing. The level of leaflet interdigitizing is small though, as apparent in the single peak observed in the methyl

group electron density profile of POPE in the Top6 membrane. The protrusion of methyl groups across the opposing bilayer's average PMPE methyl position in the Top6 membrane was calculated to be 0.5 ±1 Å. As opposed to the POPE/POPG membrane where there was no protrusion, but a space of about 0.3 ± 0.2 Å.

	POPE/POPG				Top6			
	peak1		peak2		peak1		peak2	
	μ_1	σ_1	μ_2	σ_2	μ_1	σ_1	μ_2	σ_2
phosphate	20.6	2.4	-20.5	2.4	19.0	2.3	-19.0	2.3
carbonyl	16.4	2.4	-16.3	2.4	14.8	2.3	-14.8	2.3
ring	–	–	–	–	6.8	2.8	-6.8	2.9
double bond	8.6	2.8	-8.5	2.8	7.2	3.0	-7.1	2.9
methyl	0.0	3.1	–	–	0.0	3.3	–	–

Table 4.2 Gaussian fits of EDP. All units in Å.

The K_A of the POPE/POPG and Top6 membranes were 0.25 ± 0.04 and 0.34 ± 0.04 N/m respectively, thus the Top6 membrane is more rigid than the POPE/POPG membrane. Using the CED well (Fig. 4.3) and calculating the available thermal energy to be 0.001 J/nm^2 we estimated the POPE/POPG and Top6 bilayer thickness to thermally fluctuate between 36 – 44 and 35 – 40 Å respectively.

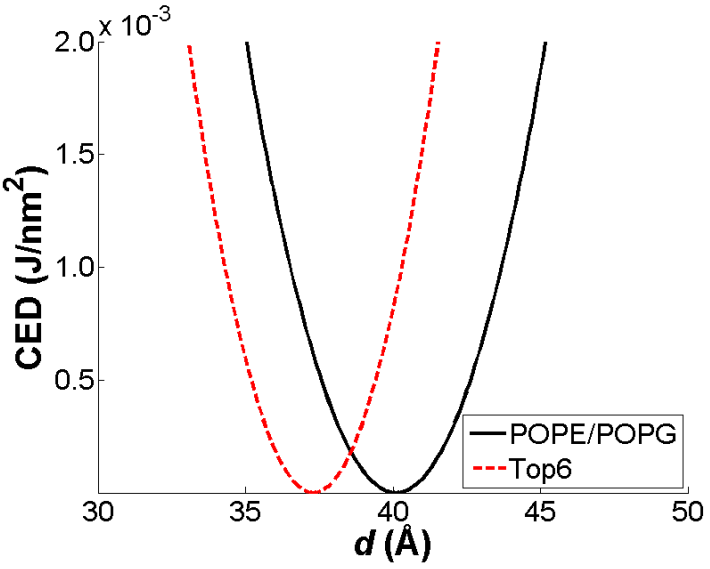

Figure 4.3 Compression energy density. The POPE/POPG (*black solid*) and Top6 (*red dashed*) membranes are likely to fluctuate between 36 – 44 and 35 – 40 Å in thickness respectively.

A summary of the Top6 and POPE/POPG membrane properties is given below.

Membrane	SA [Å^2/lipid]	Z [Å]	D [Å]	K_A [N/m]
POPE/POPG	60 ± 1	40.1 ± 0.1	32.7 ± 0.3	0.25 ± 0.04
Top6	64 ± 1	37.3 ± 0.2	29.8 ± 0.1	0.34 ± 0.04

Table 4.3 Summary of membrane properties.

CHAPTER 5 DISCUSSION AND CONCLUSION

A detailed *E. coli* membrane was developed to include a diverse set of lipids including species with a cyclic moiety. Most commonly, PE or in some cases PE/PG 18:1/16:0 lipids are used to model bacterial membranes, but the inclusion of lipids with a cyclic moiety produced noticeable changes in the surface density and stiffness of the membrane. Furthermore, the overall shorter acyl chain length of the Top6 membrane formed a thinner bilayer than the POPE/POPG membrane.

The composition of the Top6 membrane included cyclic lipids, which contain a high strain cyclopropane ring. *In vivo, E. coli* use an enzyme to add a methyl group across the double bonds of monounsaturated FAs (Grogan and Cronan 1997), which are synthesized late in the exponential growth phase. Indeed a decline of C16:1 and increase of cyC17:0 FAs during growth have been observed (Shokri and Larsson 2004). The advantage of this high energy process is to improve the fluidity of the cell membrane (Grogan and Cronan 1997; Dufourc, Smith, and Jarrell 1984; Dufourc, Smith, and Jarrell 1983; B Perly, Smith, and Jarrell 1985; Bruno Perly, Smith, and Jarrell 1985). Cyclic lipids do not pack as well as monounsaturated lipids, thus they are more likely to remain in a bilayer phase in response to perturbations and less likely to solidify into a gel phase. Also, the highly strained rings are stable in the lipid bilayer (Grogan and Cronan 1997).

Besides the inclusion of cyclopropane rings the Top6 membrane consist of a diverse set of lipids. FA chain lengths range from 15 to 18 carbons long, with the average acyl chain length of 16 carbons. Lipids with two monounsaturated chains (OSPE), one saturated and one

monounsaturated chain (POPE & PSPG) and one saturated and one cyclic chain (QMPE, PMPG, & PMPE) are represented. As observed in experiment, C16:0 is the most populous FA (Shokri and Larsson 2004; Morein et al. 1996; Ingram 1977; Oursel et al. 2007; Ishida et al. 2006). Overall, the composition accurately reflects the diversity found in *E. coli* membranes.

Initially, we attempted to use *cis* double bonded carbon parameters to describe the ring. However, inconsistencies with experimental S_{CD} parameters motivated us to develop QM-based parameters for the cyclic moiety. Our developed FF parameters more closely matched the experimental S_{CD} parameters (See Fig. 3.5). There were some slight differences such as in the splitting at key carbons, but the overall pattern agreed well. Also, taking into account the uncertainty in experiment, such as labeling acyl chains at specific carbons, we feel our QM-based parameters for the cyclic moiety are excellent.

The main difference between the S_{CD} profile between the POPE and PMPE was the brief restoration of order between C9 and C10 (See Fig. 4.1). The double bond moiety effectively kinks the chain, which creates more volume for the C-H bonds to occupy and thereby decreasing the order of the chain at double bonds. The geometry of the ring also kinks the acyl chain because it prevents rotation around the C9-C10 bond. Thus, the acyl chain order is decreased at the C9 and C10 in the cyclic moiety as well. However, the ring carbon, C17, is fixed in relation to C9 and C10 and confined to smaller volume, thereby increasing the order of the chain at the ring position.

The protruding stable carbon also increased the surface area of PMPE (See Table 4.3). In broad terms, cyclic moieties decrease the surface density of lipids much like branched lipids (Lim and Klauda 2011). A less dense bilayer could also allow for increased protein dynamics.

The protruded carbon topology of cyclic moieties may also stabilize proteins better by fitting into crevices between folds.

The hydrophobic thickness of the membrane directly influences membrane and protein interaction and the tilt of the protein in the membrane. Negative hydrophobic mismatches, when the hydrophobic length of the protein is less than the membrane, causes local lipid deformations surrounding the protein to adjust to the hydrophobic length of the tilted protein. Positive hydrophobic mismatches, the hydrophobic length of the protein is greater than the membrane, mostly influences the tilt angle of the protein only (Kim and Im 2010). A survey of *E. coli* cytosolic membrane proteins with significant transmembrane portions in the Orientations of Proteins in Membranes database (OPM) (M. A. Lomize et al. 2006) shows that the average hydrophobic thickness is 29.4 ± 1 Å. The OPM database orients (rotation, depth, and tilt) proteins in an implicit, adjustable thickness, anistropic solvent model of a lipid bilayer. The POPE/POPG membrane hydrophobic thickness is slightly greater where as the Top6 membrane agrees very well with the OPM survey (See Table 4.3).

The energetic cost associated with deforming the membrane to match the hydrophobic length is mostly to due to compression/expansion of the bilayer and bending of the monolayer. The monolayer bending modulus is a function of the lipid head group size and the PE:PG is similar in the POPE/POPG and Top6 membranes. Therefore, we assumed the energetic cost due to bending of the monolayer was similar for the POPE/POPG and Top6 membranes. The K_A is a function of the surface area per lipid of the membrane. Thus, the Top6 membrane had a larger K_A and was slightly harder to compress/expand (See Table 4.3). However, the hydrophobic thickness of the Top6 membrane matches the calculated hydrophobic length of *E. coli* transmembrane proteins so it can afford to be more rigid. The flexibility of the POPE/POPG

membrane allows for compression to match the hydrophobic length of transmembrane proteins found in *E. coli* at a minimal cost of 200 – 250 J/mol (See Figure 4.3).

The Top6 membrane will likely be beneficial in several areas of *E. coli* membrane MD research such as antimicrobial peptides (AMPs), proteins which are regulated by the membrane and integral membrane proteins which undergo large conformational changes. AMPs are membrane associated proteins which insert into the membrane to kill bacteria. It is believed that they insert into the membrane unfolded where secondary structure is then induced (Cirac et al. 2011). The insertion process, which perturbs the membrane, could be affected by the compressibility and surface area per lipid of the membrane. AMPs then kill the bacteria by permeabilizing the membrane by forming pores across the membrane, which depends on the thickness of the membrane. Cirac et al. (Cirac et al. 2011) performed MD simulations using a DPPG bilayer described by a GROMOS96 based force field to understand the molecular basis of how AMPs functions. It is very conceivable that the molecular interactions could change upon using a more accurate membrane.

The complex membrane should also be beneficial in understanding the interactions between membranes and membrane regulated proteins such as *E. coli* mechanosensitive channels (MscL and MscS). These channels serve as turgor pressure release valves and open or close in response to tension in the membrane. Wiggins and Phillips have estimated that the bilayer thickness deformation due to hydrophobic mismatching is important in gating of MscS (Wiggins and Phillips 2005). In fact, Perozo et al. performed experiments where decreasing the bilayer thickness decreased the activation energy of MscL (Perozo et al. 2002). Thus, the compressibility and thickness of the membrane help regulate the opening and closing of these channels. Explicit membrane MD studies of MscS have used POPE bilayers described by a GROMOS FF (Spronk,

Elmore, and Dougherty 2006) and POPC bilayers described by a CHARMM27 FF (Anishkin, Kamaraju, and Sukharev 2008; Sotomayor et al. 2007). The use of these simple membranes may produce artifacts which would not be seen with a more accurate membrane.

A detailed *E. coli* membrane has been developed for use in MD simulations. The composition of the bilayer was fit to a several experimentally determined compositions of *E. coli* and consisted of six different lipids, including lipids with a cyclic moiety near the center of the chain. QM-based parameters were developed to describe the cyclopropane ring within the acyl chain to match deuterium order parameters. The complex membrane was simulated along with simple POPE/POPG and pure PMPE membranes. It was found that the complex membrane matched the hydrophobic length of integral *E. coli* membrane proteins better than the POPE/POPG membrane. The complex membrane was also less dense and slightly more rigid. To our knowledge, the complex Top6 membrane is the most accurate representation of an *E. coli* cytoplasmic lipid bilayer. We believe that more accurate simulations are possible with a diverse population of lipids and suggest the use of the Top6 membrane as opposed to simple POPE or POPE/POPG membranes for MD simulations of *E. coli* membranes.

CHAPTER 6 FUTURE DIRECTIONS

6.1 Introduction

The future direction for this research is to use the Top6 membrane in simulating the full transition pathway of Mhp1, a secondary active transport protein (details presented below). In doing so we will further test the new implicit-explicit membrane method (IM-EX) developed in Dr. Klauda's lab to investigate conformational changes of integral membrane proteins without bias (Pendse, Brooks, and Klauda 2010). Additionally, the effects of a transmembrane potential on the transition pathway and the free energy of ligand binding will be investigated. Although not my future direction, others in Dr. Klauda's lab are using this to study *E. coli* transmembrane proteins and hopefully, many other investigators will find the Top6 membrane useful in their future research.

Secondary active transport proteins pump ligands across the cell membrane against their gradient by coupling the transport of ions down their chemical potential. In symporters, the ligand and ion move in the same direction across the membrane and in antiporters, the ligand and ion move in opposite directions across the membrane. Classically, the transport mechanism is described by a 6 state alternating access mechanism (Fig. 6.1, next page). The crystal structure of Mhp1 has been solved in 3 of those states; outward-facing (Weyand et al. 2008), outward-occluded with ligand and ion bound (Weyand et al. 2008), and inward-facing (Shimamura et al. 2010). Theoretically, there could be additional stable conformations that have not been identified by crystallization such an in inward-occluded state.

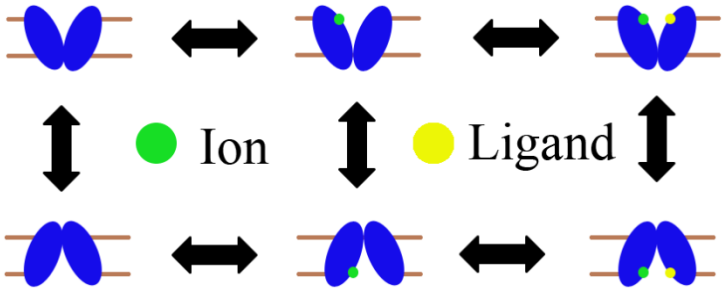

Figure 6.1 6 state alternating access mechanism. The mechanism is shown for a symporter where binding of the ion first allows for binding of the ligand.

Mhp1 is originally found in *Microbacterium liquefaciens* but was expressed and crystallized from *E. coli*. It is a symporter, coupling the transport of 1 benzyl hydantoin to 1 Na+ ion into the cell. Benzyl hydantoin is then used as a precursor to synthesize amino acids (Suzuki and Henderson 2006). Mhp1 follows an "inverted repeat" fold where 2 sets of 5 transmembrane (TM) helices are structurally very similar but one is flipped with respect to the other in the plane perpendicular to the cell membrane. Furthermore, swapping orientations between the two sets may provide a good model of the opposite conformation (Radestock and Forrest 2011). This fold is shared by several secondary active transporters such as LeuT (Yamashita et al. 2005) & vSGLT (Faham et al. 2008). The structure consists of 3 distinct rigid motifs (Fig. 6.2); the bundle

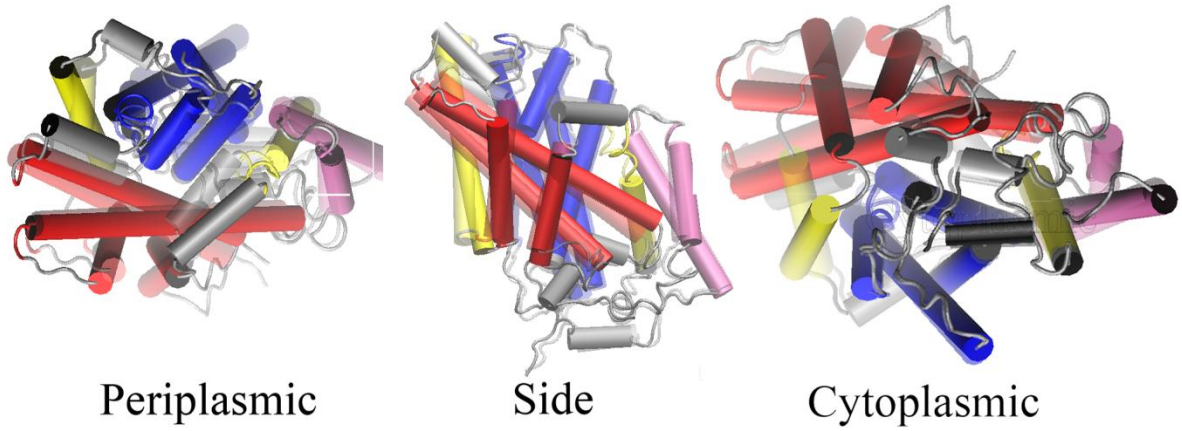

Figure 6.2 Periplasmic, side, and cytoplasmic views of Mhp1. The outward facing (*opaque*, PDB: 2JLN) and inward facing (*transparent*, PDB: 2X79) conformations are overlaid. The protein is colored as such: hash (*red*), bundle (*blue*), gates (*yellow*), c-terminal (*purple*), extracellular helices and connecting loops (*grey*).

(TM 1, 2, 6, & 7), the hash (TM 3, 4, 8, & 9), and the gates (TM 5 & 10).
There are also 2 c-terminal TM helices which, as of yet have no known function. The general conformational change mechanism follows a "rocking bundle" model (Forrest and Rudnick 2009), where the hash rocks against the bundle allowing alternate access to only the periplasm or cytoplasm. The crystal structures of the outward- and inward-facing conformations confirm the rigid body rotation of the hash as well as bending and tilting of the gates to allow for alternating access (Fig. 6.2). Additionally, the crystal structure of the occluded conformation (Not shown, PDB: 2JLO) with ligand and Na+ bound is very similar to outward conformation but shows translation of a small extracellular α-helix over the ligand and ion binding site to entrap the bound molecules.

Conformational changes of Mhp1 from one state to another have been seen in a few MD simulations. The transition from the outward-facing state to the occluded state, and then to the inward-facing state has been simulated using dynamic importance sampling (DIMS) (Shimamura et al. 2010). The DIMS simulation used an implicit membrane and solvent and did not include the ligand. In the same study equilibrium simulations with explicit solvent, explicit membrane (POPE:POPG 4:1), and ligand were also run, but only bending of the gates was observed (Shimamura et al. 2010). Recently, a coarse grain simulation was performed connecting the outward-state to the inward-state using the weighted ensemble path-sampling method (Adelman et al. 2011). The study found 2 transition pathways. One pathway further confirmed the rocking bundle alternating access and rigid body movement of the hash. The other pathway allowed for a continuous permeation pathway through the transporter. Both of these simulation methods rely on existing structures in the transition pathway in order to connect them. The IM-EX method, which we hope to test and develop, only relies on one known structure in the transport cycle. It

could be an important tool to study conformational changes of integral membrane proteins because the method is unbiased, and also there is typically only one crystal structure solved for these types of proteins.

6.2 Methods

Mhp1 will be equilibrated in a membrane by insertion into the Top6 membrane and simulated in the constant pressure, area, and temperature ensemble (NPAT) for 3 ns using P21 boundary conditions (Dolan et al. 2002). P21 boundary condition essentially transforms the lipid bilayer into one continuous layer allowing for the exchange of lipids with between layers (Fig. 6.3). Thus, if there are differences between the surface areas of a protein in each leaflet, the appropriate number of lipids in each leaflet may be chosen. The conformations between the open and closed are very similar, so the same equilibrated membrane with protein pore will be used for each initial conformation.

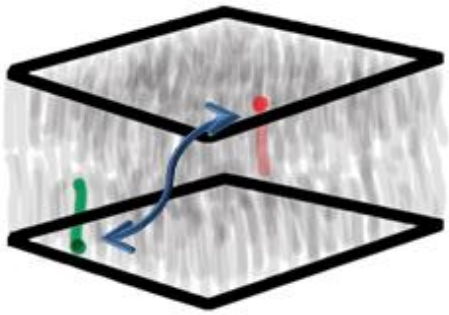

Figure 6.3 P21 boundary conditions. A lipid leaving the central box is rotated and translated so that it enters the opposite leaflet.

The two step implicit-explicit hybrid simulation approach (Pendse, Brooks, and Klauda 2010) will be used to investigate the conformational changes of Mhp1. In the first step, the protein will be simulated using self-guided Langevin dynamics (SGLD) in an implicit membrane. This will allow for enhanced conformational sampling unattainable by traditional MD. Then the trajectories will be screened for conformations in transition states to use in the

second step of simulations with the implicit Top6 *E. coli* model bilayer and implicit water. If the IM-EX method is further validated it can be used on other proteins where a structure has only been solved for on conformation.

Poisson-Boltzmann calculations were done with H++ (Gordon et al. 2005) to determine if any amino acids in Mhp1 were protonatable. It was determined that E289 could be readily protonated, thus a protonated and unprotonated state of Mhp1 will be studied. Furthermore, we would like to investigate the effect of the transmembrane potential on the transition pathway by implementing a constant electric field (Benoît Roux 2008). The transmembrane potential naturally occurs in cells from the ion gradient across the cell membrane. The potential could be important for the binding and disassociation of Na+ from Mhp1 and possible the transition of the empty carrier from the inward-facing to outward-facing. The inclusion of transmembrane potentials to study integral protein channels with MD is common, but to study secondary active transporters is unique and has not been performed before to our knowledge.

APPENDIX

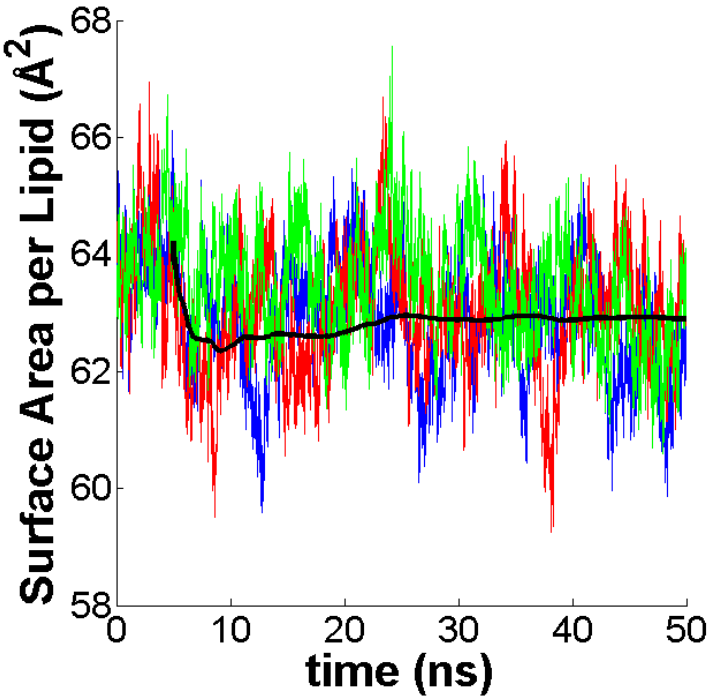

Figure A.1 Pure PMPE surface area per lipid over time. Runs 1 (*blue*), 2 (*red*), and 3 (*green*) are plotted, as well as the cumulative average (*black*) from 5 ns.

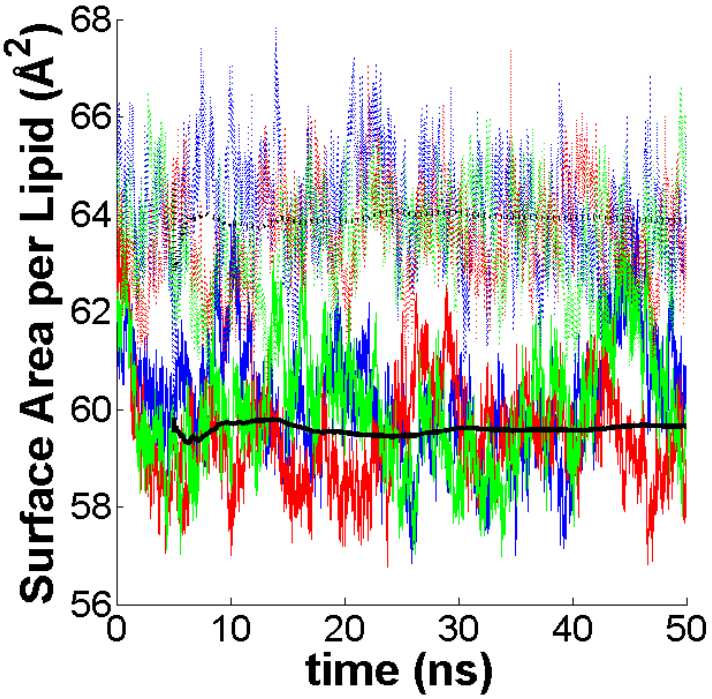

Figure A.2 Top6 & POPE/POPG surface area per lipid over time. The runs are colored as in Figure A.1. The Top6 membrane (*dotted*) is less dense than the POPE/POPG membrane (*solid*).

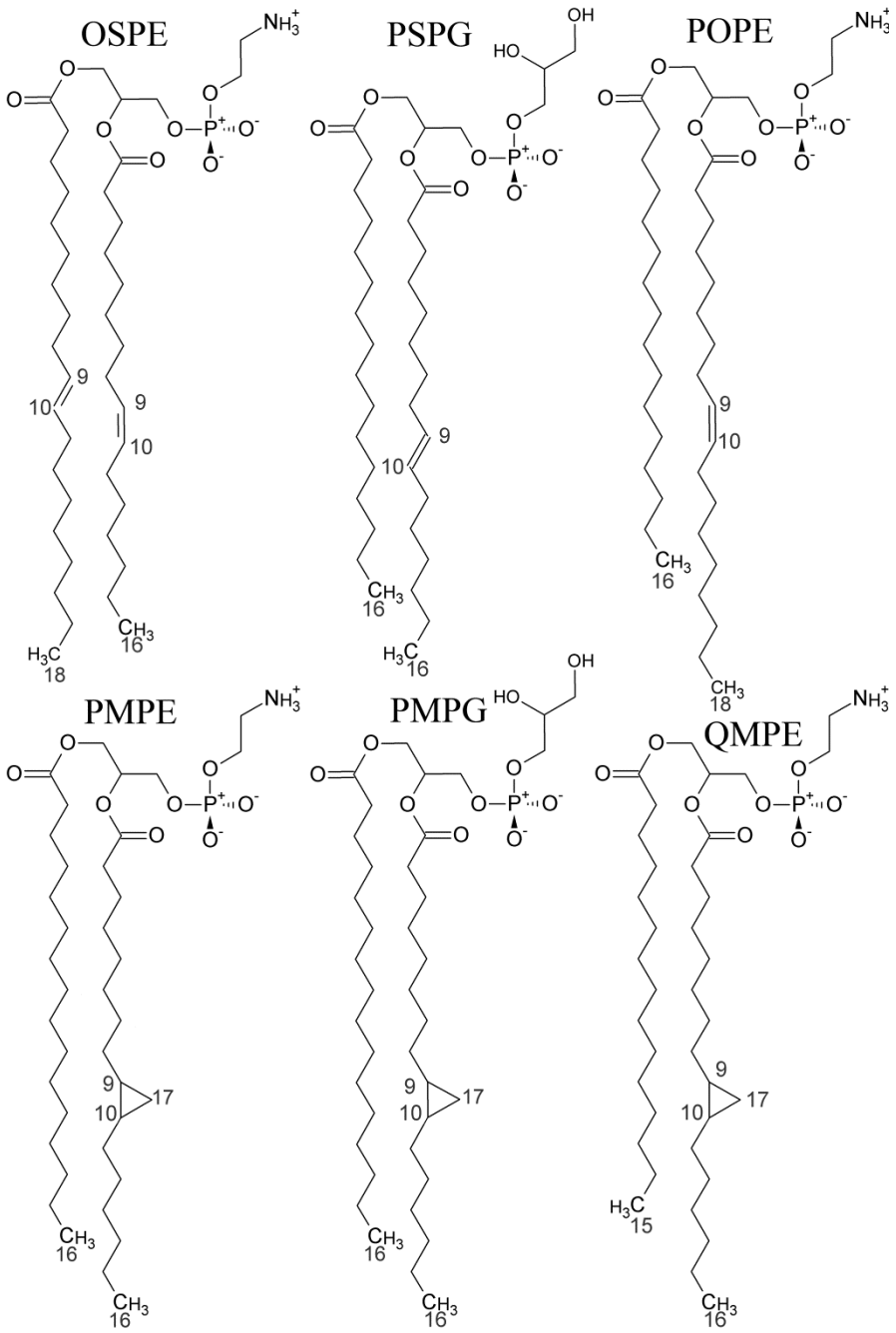

Figure A.3 Structure of Top6 lipids. The top row contains the lipids with monounsaturated acyl chains: OSPE, PSPG, and POPE. The bottom row contains the lipids with ring acyl chains: PMPE, PMPG, and QMPE. Key carbons are numbered.

Cyclic Moiety FF

```
BONDS
CTL2 CG3RC1 222.500     1.530   ! alkanes, 3/92
CG3RC1 HGA1 309.00      1.1110  ! propane ring, MacKerell
CG3RC1 CG3RC1 222.50    1.5230  ! propane ring, MacKerell
CG3C31 CG3RC1 222.50    1.5240  ! propane ring, MacKerell
CG3C31 HGA2   340.00    1.0830  ! PROTMOD cypropane, MacKerell
CG3C31 HGA1    340.00     1.0830 ! PROTMOD cyclopropane, from genFF
CTL2  CG3C31  240.00     1.5010 ! PROTMOD cyclopropane, from genFF
! Take from C36 Gen FF for Ring on small molecule studies
CTL3  CG3RC1  222.50     1.5380 ! BAM1, bile acid steroidal C-D ring, cacha, 02/08, from genFF
CTL3  CG3C31  240.00     1.5010 ! PROTMOD cyclopropane, taken from CG321 CG3C31, genFF

ANGLES
CTL2 CG3RC1 HGA1 34.50     110.10   22.53 2.179  ! propane ring, MacKerell
CG3C31 CG3RC1 HGA1 34.50   110.10   22.53  2.179 ! propane ring, MacKerell
CG3RC1 CG3C31 HGA2  34.50  110.10   22.53 2.179 ! propane ring, MacKerell
HGA2   CG3C31 HGA2  23.00  117.00   5.40  1.80200 ! PROTMOD cyclopropane MacKerell
CG3C31 CG3RC1 CG3RC1 53.35 62.50 ! propane ring, MacKerell
CG3RC1 CG3C31 CG3RC1 53.35 58.50 ! propane ring, MacKerell
CTL2 CTL2 CG3RC1 53.35    111.00    8.0   2.561 ! propane ring, MacKerell
HAL2 CTL2 CG3RC1 34.50    110.10   22.53 2.179 ! propane ring, MacKerell
CTL2 CG3RC1 CG3C31 53.35    111.00    8.0   2.561 ! propane ring, MacKerell
CTL2 CG3RC1 CG3RC1 53.35    111.00    8.0   2.561 ! propane ring, MacKerell
HGA1 CG3RC1 CG3RC1 34.50    110.10   22.53 2.179  ! propane ring, MacKerell
! Take from C36 Gen FF for Ring on small molecule studies
CG3RC1 CTL3  HAL3     33.43    110.10   22.53   2.179 ! BAM1, bile acid steroidal C-D ring,
cacha, 02/08, from GenFF
CTL3  CG3RC1 CG3RC1   58.35    113.50   11.16   2.561 ! BAM1, bile acid steroidal C-D ring,
cacha, 02/08, from GenFF
CTL3  CG3RC1 HGA1     34.50    110.10   22.53 2.179  ! CARBOCY carbocyclic sugars, taken from
CG321-CG3RC1-HGA1, from GenFF
CTL3  CG3RC1 CG3C31   53.35    111.00    8.0   2.561 ! CARBOCY carbocyclic sugars, taken from
CG321-CG3RC1-HGA1, from GenFF
CG3C31 CG3C31 HGA1     23.00    117.10   22.53  2.17900 ! PROTMOD cyclopropane, from genFF
CG3C31 CG3C31 CG3C31   77.35    111.00    8.00  2.56100 ! PROTMOD cyclopropane, from genFF
CG3C31 CG3C31 HGA2     23.00    117.10   22.53  2.17900 ! PROTMOD cyclopropane, from genFF
CG3C31 CTL2   HAL2     26.50    110.10   22.53   2.17900 ! PROT alkane update, adm jr., 3/2/92,
from genFF

DIHEDRALS
HAL2   CTL2   CG3RC1 HGA1   0.1500  3     0.00 ! propane ring, MacKerell
HGA2   CG3C31 CG3RC1 HGA1   0.1500  3     0.00 ! propane ring, MacKerell
HGA1   CG3RC1 CG3RC1 HGA1   0.1500  3     0.00 ! propane ring, MacKerell
CTL2   CTL2   CG3RC1 HGA1   0.1500  3     0.00 ! propane ring, MacKerell
CTL2   CTL2   CG3RC1 CG3C31 0.0000  2   180.00 ! propane ring, MacKerell
HGA2   CG3C31 CG3RC1 CTL2   0.1950  3     0.00 ! propane ring, MacKerell
CG3RC1 CG3C31 CG3RC1 CTL2   0.1500  3     0.00 ! propane ring, MacKerell
CTL2   CG3RC1 CG3RC1 CG3C31 0.1500  3     0.00 ! propane ring, MacKerell
CTL2   CG3RC1 CG3RC1 HGA1   0.1500  3     0.00 ! propane ring, MacKerell
CTL2   CG3RC1 CG3RC1 CTL2   0.1500  3     0.00 ! propane ring, MacKerell
HAL2   CTL2   CG3RC1 CG3C31 0.1950  3     0.00 ! propane ring, MacKerell
HAL2   CTL2   CG3RC1 CG3RC1 0.1500  3     0.00 ! propane ring, MacKerell
CG3RC1 CG3C31 CG3RC1 HGA1   0.1500  3     0.00 ! propane ring, MacKerell
HGA2   CG3C31 CG3RC1 CG3RC1 0.1500  3     0.00 ! propane ring, MacKerell
CG3C31 CG3RC1 CG3RC1 HGA1   0.1500  3     0.00 ! propane ring, MacKerell
! Take from C36 Gen FF for Ring on small molecule studies
CG3RC1 CG3C31 CG3RC1 CTL3   0.1500  3     0.00 ! CARBOCY carbocyclic sugars, taken from CG3RC1
CG3C31 CG3RC1 CG321, genFF
HGA2   CG3C31 CG3RC1 CTL3   0.1950  3     0.00 ! CARBOCY carbocyclic sugars, taken from HGA2
CG3C31 CG3RC1 CG321, genFF
HAL3   CTL3   CG3RC1 CG3RC1 0.1500  3   180.00 ! BAM1, bile acid steroidal C-D ring, cacha, 02/08
HAL3   CTL3   CG3RC1 HGA1   0.1600  3     0.00 ! alkane, 4/98, yin and mackerell, tf2m viv, taken
from HGA3 CG331 CG3C51 HGA1, genFF
HAL3   CTL3   CG3RC1 CG3C31 0.1500  3   180.00 ! BAM1, bile acid steroidal C-D ring, cacha,
02/08, taken from HGA3 CG331 CG3RC1 CG3C51, genFF
```

```
CG3RC1 CTL2 CTL2 CTL3     0.1400  1    180.0 !2-hexene, adm jr., 11/09 from C36 GenFF
CG3RC1 CTL2 CTL2 CTL3     0.1700  2      0.0 !2-hexene, adm jr., 11/09 from C36 GenFF
CG3RC1 CTL2 CTL2 CTL3     0.0500  3    180.0 !2-hexene, adm jr., 11/09 from C36 GenFF
CG3RC1 CG3RC1 CTL2 CTL2     1.71  1    159.6 !ring, KRP
CG3RC1 CG3RC1 CTL2 CTL2     0.37  2    165.1 !ring, KRP
CG3RC1 CG3RC1 CTL2 CTL2     0.58  3     47.6 !ring, KRP
CG3RC1 CTL2 CTL2 CTL2     0.16  1    180.0 ! ring, KRP
CG3RC1 CTL2 CTL2 CTL2     0.01  2    180.0 ! ring, KRP
CG3RC1 CTL2 CTL2 CTL2     0.17  3    180.0 ! ring, KRP

NONBONDED nbxmod  5 atom cdiel fshift vatom vdistance vfswitch -
cutnb 14.0 ctofnb 12.0 ctonnb 10.0 eps 1.0 e14fac 1.0 wmin 1.5
HGA1    0.0       -0.0450     1.3400 ! alkane, igor, 6/05
HGA2    0.0       -0.0350     1.3400 ! alkane, igor, 6/05
CG3RC1 0.0        -0.0320     2.0000   0.0 -0.01 1.9 ! alkane (CT1), viv
CG3C31   0.0        -0.0560     2.0100   0.0 -0.01 1.9 ! cyclopropane JMW (CT2), viv
```

The parameterized dihedrals terms are highlighted.

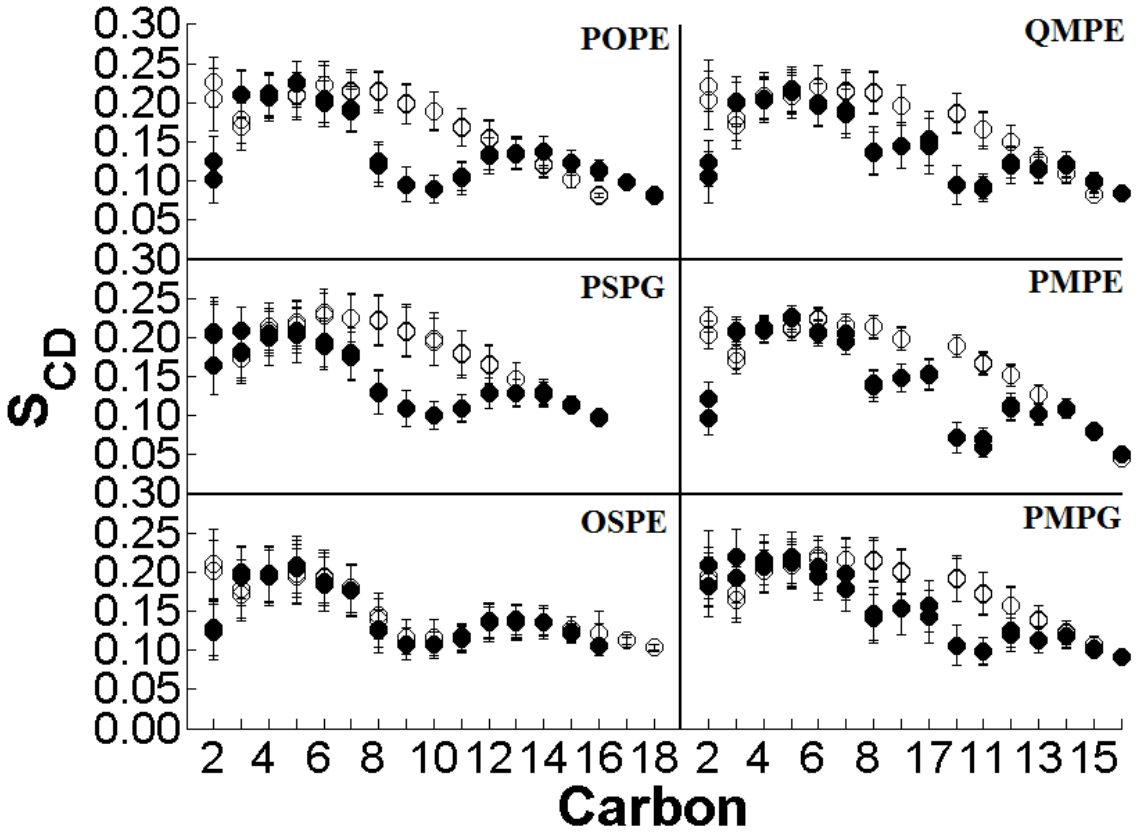

Figure A.4 S_{CD} profile of Top6 lipids. The *sn*-1 acyl chain is shown in open circles and the *sn*-2 acyl chain is shown filled circles. Lipids with double bonds are shown on the left, and lipids with rings are shown on the right. The same double bond and ring induced disordering pattern is seen in the respective lipids. At the 2nd carbon position, the *sn*-1 carbons are more ordered than the *sn*-2 carbons for PE lipids. In PG lipids at the 2nd carbon position, the carbons are of the same order, irrespective of the chain.

REFERENCES

Adelman, Joshua L., Amy L. Dale, Matthew C. Zwier, Divesh Bhatt, Lillian T. Chong, Daniel M. Zuckerman, and Michael Grabe. 2011. "Simulations of the Alternating Access Mechanism of the Sodium Symporter Mhp1." *Biophysical Journal* 101 (November): 2399-2407. Laptop. doi:10.1016/j.bpj.2011.09.061.

Alhadeff, Raphael, Assaf Ganoth, Miriam Krugliak, and Isaiah T. Arkin. 2011. "Promiscuous Binding in a Selective Protein: The Bacterial Na+/H+ Antiporter." *PLoS ONE* 6 (10) (October 12): e25182. Laptop. doi:10.1371/journal.pone.0025182.

Anishkin, Andriy, Kishore Kamaraju, and Sergei Sukharev. 2008. "Mechanosensitive Channel MscS in the Open State: Modeling of the Transition, Explicit Simulations, and Experimental Measurements of Conductance." *The Journal of General Physiology* 132 (1) (July 1): 67 -83. UMD. doi:10.1085/jgp.200810000.

Brooks, B R, C L Brooks 3rd, A D Mackerell Jr, L Nilsson, R J Petrella, B Roux, Y Won, et al. 2009. "CHARMM: the biomolecular simulation program." *Journal of Computational Chemistry* 30 (10) (July 30): 1545-1614. Online. doi:10.1002/jcc.21287.

Burnett, L. J. 1971. "Deuteron Quadrupole Coupling Constants in Three Solid Deuterated Paraffin Hydrocarbons: C2D6, C4D10, C6D14." *The Journal of Chemical Physics* 55 (12): 5829. Laptop. doi:10.1063/1.1675758.

Cirac, Anna D., Gemma Moiset, Jacek T. Mika, Armagan Koc¸er, Pedro Salvador, Bert Poolman, Siewert J. Marrink, and Durba Sengupta. 2011. "The Molecular Basis for Antimicrobial Activity of Pore-FormingCyclic Peptides." *Biophysical Journal* 100 (10) (May): 2422-2431. Laptop. doi:10.1016/j.bpj.2011.03.057.

Dalrymple, O.K., W. Isaacs, E. Stefanakos, M.A. Trotz, and D.Y. Goswami. 2011. "Lipid vesicles as model membranes in photocatalytic disinfection studies." *Journal of Photochemistry and Photobiology A: Chemistry* 221 (1) (June 10): 64-70. UMD. doi:16/j.jphotochem.2011.04.025.

Darden, Tom, Darrin York, and Lee Pedersen. 1993. "Particle mesh Ewald: An N·log(N) method for Ewald sums in large systems." *The Journal of Chemical Physics* 98 (12): 10089. Online. doi:10.1063/1.464397.

Dolan, Elizabeth A., Richard M. Venable, Richard W. Pastor, and Bernard R. Brooks. 2002. "Simulations of Membranes and Other Interfacial Systems Using P21 and Pc Periodic Boundary Conditions." *Biophysical Journal* 82 (5) (May): 2317-2325. doi:10.1016/S0006-3495(02)75577-X.

Dombek, K. M, and L. O. Ingram. 1984. "Effects of ethanol on the Escherichia coli plasma membrane." *Journal of bacteriology* 157 (1): 233. Laptop.

Dufourc, Erick J., Ian C. P. Smith, and Harold C. Jarrell. 1984. "The role of cyclopropane moieties in the lipid properties of biological membranes: a deuterium NMR structural and dynamical approach." *Biochemistry* 23 (10) (May 1): 2300-2309. UMD. doi:10.1021/bi00305a033.

Dufourc, Erick J., Ian C.P. Smith, and Harold C. Jarrell. 1983. "A 2H-NMR analysis of dihydrosterculoyl-containing lipids in model membranes: structural effects of a cyclopropane ring." *Chemistry and Physics of Lipids* 33 (2) (August): 153-177. HardCopy. doi:16/0009-3084(83)90019-1.

Faham, Salem, Akira Watanabe, Gabriel Mercado Besserer, Duilio Cascio, Alexandre Specht, Bruce A. Hirayama, Ernest M. Wright, and Jeff Abramson. 2008. "The Crystal Structure

of a Sodium Galactose Transporter Reveals Mechanistic Insights into Na+/Sugar Symport." *Science* 321 (5890): 810 -814. doi:10.1126/science.1160406.
Feller, Scott E., Yuhong Zhang, Richard W. Pastor, and Bernard R. Brooks. 1995. "Constant pressure molecular dynamics simulation: The Langevin piston method." *The Journal of Chemical Physics* 103 (11): 4613. doi:10.1063/1.470648.
Forrest, Lucy R., and Gary Rudnick. 2009. "The Rocking Bundle: A Mechanism for Ion-Coupled Solute Flux by Symmetrical Transporters." *Physiology* 24 (6) (December 1): 377 -386. doi:10.1152/physiol.00030.2009.
Frisch, M. J., G. W. Trucks, H. B. Schlegel, G. E. Scuseria, M. A. Robb, J. R. Cheeseman, J. A. Montgomery, Jr., et al. 2003. *Gaussian 03*. Pittsburgh, PA: Gaussian, Inc.
Gordon, John C., Jonathan B. Myers, Timothy Folta, Valia Shoja, Lenwood S. Heath, and Alexey Onufriev. 2005. "H++: a server for estimating pKas and adding missing hydrogens to macromolecules." *Nucleic Acids Research* 33 (Web Server issue) (July 1): W368-W371. doi:10.1093/nar/gki464.
Grogan, DW, and JE Cronan. 1997. "Cyclopropane ring formation in membrane lipids of bacteria." *Microbiol. Mol. Biol. Rev.* 61 (4) (December 1): 429-441. UMD. doi: .
Guvench, Olgun, and Alexander D. MacKerell. 2008. "Automated conformational energy fitting for force-field development." *Journal of Molecular Modeling* 14 (May 6): 667-679. Laptop. doi:10.1007/s00894-008-0305-0.
Hoover, William G. 1985. "Canonical dynamics: Equilibrium phase-space distributions." *Physical Review A* 31 (3) (March 1): 1695. Online. doi:10.1103/PhysRevA.31.1695.
Ingram, L O. 1977. "Changes in lipid composition of Escherichia coli resulting from growth with organic solvents and with food additives." *Applied and Environmental Microbiology* 33 (5) (May): 1233-1236. UMD.
Ishida, Yasuyuki, Kuniyuki Kitagawa, Akihito Nakayama, and Hajime Ohtani. 2006. "Complementary analysis of lipids in whole bacteria cells by thermally assisted hydrolysis and methylation-GC and MALDI-MS combined with on-probe sample pretreatment." *Journal of Analytical and Applied Pyrolysis* 77 (2) (October): 116-120. UMD. doi:16/j.jaap.2006.02.006.
Jo, S., T. Kim, V.G. Iyer, and W. Im. 2008. CHARMM-GUI: A web-based graphical user interface for CHARMM. Journal of Computational Chemistry. 29: 1859-1865.
Jo, Sunhwan, Joseph B. Lim, Jeffery B. Klauda, and Wonpil Im. 2009. "CHARMM-GUI Membrane Builder for Mixed Bilayers and Its Application to Yeast Membranes." *Biophysical Journal* 97 (1) (July 8): 50-58. Online. doi:10.1016/j.bpj.2009.04.013.
Kim, Taehoon, and Wonpil Im. 2010. "Revisiting Hydrophobic Mismatch with Free Energy Simulation Studies of Transmembrane Helix Tilt and Rotation." *Biophysical Journal* 99 (1) (July 7): 175-183. Thumbdrive, Laptop. doi:16/j.bpj.2010.04.015.
Klauda, Jeffery B., Stephen L. Garrison, Jianwen Jiang, Gaurav Arora, and Stanley I. Sandler. 2003. "HM-IE: Quantum Chemical Hybrid Methods for Calculating Interaction Energies." *J. Phys. Chem. A* 108 (1): 107-112. doi:10.1021/jp035639e.
Klauda, Jeffery B., Richard M. Venable, J. Alfredo Freites, Joseph W. O'Connor, Douglas J. Tobias, Carlos Mondragon-Ramirez, Igor Vorobyov, Alexander D. MacKerell, and Richard W. Pastor. 2010. "Update of the CHARMM All-Atom Additive Force Field for Lipids: Validation on Six Lipid Types." *The Journal of Physical Chemistry B* 114 (23) (June 17): 7830-7843. UMD. doi:10.1021/jp101759q.

Krämer, R., and C. Ziegler. 2009. “Regulative interactions of the osmosensing C-terminal domain in the trimeric glycine betaine transporter BetP from Corynebacterium glutamicum.” *Biological Chemistry* 390 (8): 685–691. UMD.

Leach, Andrew. 2001. *Molecular Modelling Principles and Applications*. 2nd ed. Harlow, England; New York: Prentice Hall.

Lensink, Marc F., Cédric Govaerts, and Jean-Marie Ruysschaert. 2010. “Identification of Specific Lipid-binding Sites in Integral Membrane Proteins.” *Journal of Biological Chemistry* 285 (14) (April 2): 10519 -10526. Thumbdrive, Laptop. doi:10.1074/jbc.M109.068890.

Letellier, L, H Moudden, and E Shechter. 1977. “Lipid and protein segregation in Escherichia coli membrane: morphological and structural study of different cytoplasmic membrane fractions.” *Proceedings of the National Academy of Sciences* 74 (2) (February 1): 452 - 456. UMD.

Lim, Joseph B., and Jeffery B. Klauda. 2011. “Lipid chain branching at the iso- and anteiso-positions in complex chlamydia membranes: A molecular dynamics study.” *Biochimica et Biophysica Acta (BBA) - Biomembranes* 1808 (1) (January): 323-331. Laptop, Thumbdrive. doi:16/j.bbamem.2010.07.036.

Lomize, Mikhail A, Andrei L Lomize, Irina D Pogozheva, and Henry I Mosberg. 2006. “OPM: orientations of proteins in membranes database.” *Bioinformatics (Oxford, England)* 22 (5) (March 1): 623-625. Online. doi:10.1093/bioinformatics/btk023.

McAuley, Katherine E., Paul K. Fyfe, Justin P. Ridge, Neil W. Isaacs, Richard J. Cogdell, and Michael R. Jones. 1999. “Structural details of an interaction between cardiolipin and an integral membrane protein.” *Proceedings of the National Academy of Sciences* 96 (26) (December 21): 14706 -14711. doi:10.1073/pnas.96.26.14706.

Mileykovskaya, Eugenia, and William Dowhan. 2000. “Visualization of Phospholipid Domains in Escherichia coli by Using the Cardiolipin-Specific Fluorescent Dye 10-N-Nonyl Acridine Orange.” *J. Bacteriol.* 182 (4) (February 15): 1172-1175. Thumbdrive, Laptop. doi: 10.1128/JB.182.4.1172-1175.2000 .

Morein, Sven, Ann-Sofie Andersson, Leif Rilfors, and Göran Lindblom. 1996. “Wild-type Escherichia coli Cells Regulate the Membrane Lipid Composition in a Window between Gel and Non-lamellar Structures.” *Journal of Biological Chemistry* 271 (12) (March 22): 6801 -6809. UMD. doi:10.1074/jbc.271.12.6801.

Murzyn, K, and M Pasenkiewicz-Gierula. 1999. “Construction and optimisation of a computer model for a bacterial membrane.” *Acta Biochimica Polonica* 46 (3): 631-639. UMD.

Nosé, Shuichi. 1983. “A study of solid and liquid carbon tetrafluoride using the constant pressure molecular dynamics technique.” *The Journal of Chemical Physics* 78 (11): 6928. doi:10.1063/1.444641.

Oursel, Delphine, Corinne Loutelier-Bourhis, Nicole Orange, Sylvie Chevalier, Victor Norris, and Catherine M Lange. 2007. “Lipid composition of membranes of Escherichia coli by liquid chromatography/tandem mass spectrometry using negative electrospray ionization.” *Rapid Communications in Mass Spectrometry* 21 (11) (June 15): 1721-1728. UMD. doi:10.1002/rcm.3013.

Pendse, Pushkar Y., Bernard R. Brooks, and Jeffery B. Klauda. 2010. “Probing the Periplasmic-Open State of Lactose Permease in Response to Sugar Binding and Proton Translocation.” *Journal of Molecular Biology* 404 (3) (December 3): 506-521. Thumbdrive, Laptop. doi:16/j.jmb.2010.09.045.

Perly, B, I C Smith, and H C Jarrell. 1985. “Acyl chain dynamics of phosphatidylethanolamines containing oleic acid and dihydrosterculic acid: 2H NMR relaxation studies.” *Biochemistry* 24 (17) (August 13): 4659-4665. Online.

Perly, Bruno, Ian C. P. Smith, and Harold C. Jarrell. 1985. “Effects of the replacement of a double bond by a cyclopropane ring in phosphatidylethanolamines: a deuterium NMR study of phase transitions and molecular organization.” *Biochemistry* 24 (4) (February 1): 1055-1063. Hard Copy. doi:10.1021/bi00325a038.

Perozo, Eduardo, Anna Kloda, D. Marien Cortes, and Boris Martinac. 2002. “Physical principles underlying the transduction of bilayer deformation forces during mechanosensitive channel gating.” *Nat Struct Mol Biol* 9 (9): 696-703. Laptop. doi:10.1038/nsb827.

Phillips, James C, Rosemary Braun, Wei Wang, James Gumbart, Emad Tajkhorshid, Elizabeth Villa, Christophe Chipot, Robert D Skeel, Laxmikant Kalé, and Klaus Schulten. 2005. “Scalable molecular dynamics with NAMD.” *Journal of Computational Chemistry* 26 (16) (December 1): 1781-1802. Online. doi:10.1002/jcc.20289.

Popot, Jean-Luc. 2010. “Amphipols, Nanodiscs, and Fluorinated Surfactants: Three Nonconventional Approaches to Studying Membrane Proteins in Aqueous Solutions.” *Annual Review of Biochemistry* 79 (1) (June): 737-775. UMD. doi:10.1146/annurev.biochem.052208.114057.

Radestock, Sebastian, and Lucy R. Forrest. 2011. “The Alternating-Access Mechanism of MFS Transporters Arises from Inverted-Topology Repeats.” *Journal of Molecular Biology* 407 (5) (April 15): 698-715. doi:10.1016/j.jmb.2011.02.008.

Razin, S. 1975. “Cholesterol incorporation into bacterial membranes.” *Journal of Bacteriology* 124 (1) (October 1): 570 -572. UMD.

Roux, Benoît. 2008. “The Membrane Potential and its Representation by a Constant Electric Field in Computer Simulations.” *Biophysical Journal* 95 (9) (November 1): 4205-4216. UMD. doi:10.1529/biophysj.108.136499.

Ryckaert, Jean-Paul, Giovanni Ciccotti, and Herman J. C. Berendsen. 1977. “Numerical integration of the cartesian equations of motion of a system with constraints: molecular dynamics of n-alkanes.” *Journal of Computational Physics* 23 (3) (March): 327-341. Online. doi:16/0021-9991(77)90098-5.

Shimamura, Tatsuro, Simone Weyand, Oliver Beckstein, Nicholas G. Rutherford, Jonathan M. Hadden, David Sharples, Mark S. P. Sansom, So Iwata, Peter J. F. Henderson, and Alexander D. Cameron. 2010. “Molecular Basis of Alternating Access Membrane Transport by the Sodium-Hydantoin Transporter Mhp1.” *Science* 328 (5977) (April 23): 470 -473. Laptop, Thumbdrive. doi:10.1126/science.1186303.

Shokri, Atefeh, and Gen Larsson. 2004. “Characterisation of the Escherichia coli membrane structure andfunction during fedbatch cultivation.” *Microbial Cell Factories* 3 (9). UMD. doi:10.1186/1475-2859-3-9.

Sotomayor, Marcos, Valeria Vásquez, Eduardo Perozo, and Klaus Schulten. 2007. “Ion Conduction through MscS as Determined by Electrophysiology and Simulation.” *Biophysical Journal* 92 (3) (February 1): 886-902. Laptop. doi:29/biophysj.106.095232.

Spronk, Steven A., Donald E. Elmore, and Dennis A. Dougherty. 2006. “Voltage-Dependent Hydration and Conduction Properties of the Hydrophobic Pore of the Mechanosensitive Channel of Small Conductance.” *Biophysical Journal* 90 (10) (May 15): 3555-3569. UMD. doi:10.1529/biophysj.105.080432.

Suzuki, Shun'ichi, and Peter J. F. Henderson. 2006. "The Hydantoin Transport Protein from Microbacterium liquefaciens." *Journal of Bacteriology* 188 (9) (May 1): 3329 -3336. doi:10.1128/JB.188.9.3329-3336.2006.

US EPA. Escherichia coli K-12 Derivatives Final Risk Assessment | Biotechnology Program Under Toxic Substances Control Act (TSCA) | US EPA. http://epa.gov/biotech_rule/pubs/fra/fra004.htm.

Vanommeslaeghe, K., E. Hatcher, C. Acharya, S. Kundu, S. Zhong, J. Shim, E. Darian, et al. 2010. "CHARMM general force field: A force field for drug-like molecules compatible with the CHARMM all-atom additive biological force fields." *Journal of Computational Chemistry* 31 (4) (March 1): 671-690. doi:10.1002/jcc.21367.

Weyand, Simone, Tatsuro Shimamura, Shunsuke Yajima, Shun'ichi Suzuki, Osman Mirza, Kuakarun Krusong, Elisabeth P. Carpenter, et al. 2008. "Structure and Molecular Mechanism of a Nucleobase–Cation–Symport-1 Family Transporter." *Science* 322 (5902) (October 31): 709 -713. Thumbdrive, Laptop. doi:10.1126/science.1164440.

Wiggins, Paul, and Rob Phillips. 2005. "Membrane-Protein Interactions in Mechanosensitive Channels." *Biophysical Journal* 88 (2) (February): 880-902. Laptop. doi:10.1529/biophysj.104.047431.

Yamashita, Atsuko, Satinder K. Singh, Toshimitsu Kawate, Yan Jin, and Eric Gouaux. 2005. "Crystal structure of a bacterial homologue of Na+/Cl--dependent neurotransmitter transporters." *Nature* 437 (7056): 215-223. doi:10.1038/nature03978.

Zhao, Wei, Tomasz Róg, Andrey A. Gurtovenko, Ilpo Vattulainen, and Mikko Karttunen. 2007. "Role of phosphatidylglycerols in the stability of bacterial membranes." *Biophysical Journal* 92 (6) (February): 1114-1124. UMD. doi:10.1529/biophysj.106.086272.